Copyright Undertaking

This thesis is protected by copyright, with all rights reserved.

By reading and using the thesis, the reader understands and agrees to the following terms:

1. The reader will abide by the rules and legal ordinances governing copyright regarding the use of the thesis.
2. The reader will use the thesis for the purpose of research or private study only and not for distribution or further reproduction or any other purpose.
3. The reader agrees to indemnify and hold the University harmless from and against any loss, damage, cost, liability or expenses arising from copyright infringement or unauthorized usage.

IMPORTANT

If you have reasons to believe that any materials in this thesis are deemed not suitable to be distributed in this form, or a copyright owner having difficulty with the material being included in our database, please contact lbsys@polyu.edu.hk providing details. The Library will look into your claim and consider taking remedial action upon receipt of the written requests.

Pao Yue-kong Library, The Hong Kong Polytechnic University, Hung Hom, Kowloon, Hong Kong

http://www.lib.polyu.edu.hk

The Hong Kong Polytechnic University

Department of Applied Physics

Aluminium Nitride Nanowires for Electronic and Photonic Applications

Hui Yeung Yu

A thesis submitted in partial fulfillment of the requirements for the degree of Master of Philosophy

August 2010

Certificate of Originality

I hereby declare that this thesis is my own work and that, to the best of my knowledge and belief, it reproduces no material previously published or written nor material which has been accepted for the award of any other degree or diploma, except where due acknowledgement has been made in the text.

____________________ (Signature)

Hui Yeung Yu (Name of candidate)

Abstract

Aluminium nitride (AlN) has attracted particular research enthusiasm for their promising application as short wavelength light emission devices and high power transistors. AlN has the largest band gap of ~6.0 eV among all the group III nitrides, and has excellent thermal, mechanical and chemical stability, and low electron affinity. It is a promising candidate for deep-ultraviolet (DUV) light emitting devices. DUV light sources have attracted considerable attention because of their potential uses in environmental protection equipment, nano-fabrication technology, high-density optical data storage, water and air purification, and sterilization.

Semiconductor nanowires have been demonstrated significant potential as fundamental building blocks for nanoelectronics and nanophotonic devices. As compared to AlN epilayers, one-dimensional (1D) AlN nanostructures have the following appealing features: They can be single-crystalline, relatively defect-free, having atomically smooth surfaces and able to accommodate large lattice mismatch. In this work, we investigate the synthesis and characterization of AlN nanowires and pay particular attention in preparing Mg-doped AlN nanowires (AlNNWs). Mg is a potential *p*-type dopant for AlN. It is predicted that Mg could also be doped into AlN to make it ferromagnetic.

AlNNWs and zigzag AlNNWs were synthesized by chemical vapor deposition. Randomly aligned nanowires and zigzag nanowires with single-crystalline structure were synthesized on sapphire substrates at 1450 °C and 1350 °C respectively under the

flow of nitrogen (N_2) gas. It is found that when the substrate was located at a low temperature zone, it was relatively easier to dope Mg into the nanowires and the growth of zigzag nanowires was imitated. The structural, magnetic and optical properties of the nanowires and zigzag nanowires were characterized by X-ray diffraction (XRD), Raman spectroscopy, scanning electron microscopy (SEM), transmission electron microscopy (TEM), vibrating sample magnetometer (VSM) cathodoluminescence (CL) and photoluminescence (PL).

The high resolution transmission electron microscopy (HR-TEM) and the selected area electron diffraction (SAED) revealed that the nanowires were single crystalline, with the lattice spacing matched wurtzite hexagonal AlN (h-AlN). The growth axis of the nanowires was identified to be the hexagonal *a*-axis along the [100] direction. As detected by the energy-dispersive X-ray spectroscopy (EDX), the nanowires contained no Mg dopant. The diameter and length of the nanowires were ranging from 20 nm to 100 nm and 10 μm to 50 μm, respectively. Two vibration modes A_1 (TO) and E_2 (high) located at 612 and 656 cm^{-1} respectively were observed from the Raman spectrum, which fitted well with the stress-free bulk AlN crystal. Room temperature CL showed a strong and broad emission peaked at around 3.50 eV. Room temperature PL spectrum also showed a similar emission peak at around 3.51 eV when the samples were excited by a quadrupled Ti-sapphire femtosecond laser (195 nm). The emission was attributed to oxygen substituting the nitrogen vacancy (O_N).

The HR-TEM images and the SAED patterns revealed that the zigzag nanowires were also single crystalline, with the lattice spacing matched wurtzite h-AlN. The growth axis

of the zigzag nanowires was identified to be the hexagonal *c*-axis along the [001] direction. About 5 at.% of Mg was estimated in the zigzag nanowire. The diameter and length of the nanowires were ranging from 50 nm to 100 nm and 10 μm to 50 μm, respectively. Slight redshift of the two vibration modes A_1 (TO) and E_2 (high) located at 616 and 660 cm^{-1} respectively were observed from the Raman spectrum, which could be attributed by the incorporation of Mg. It is noted that ferromagnetic properties can be obtained only from the zigzag nanowires. The spontaneous saturated magnetization and coercivity measured in the magnetization versus magnetic field *(M-H)* loop of the zigzag nanowires were estimated to be ~50 μemu/cm^2 and 3 kOe respectively when the field was applied perpendicular to the sample. Both room temperature CL and PL spectrum showed a strong and broad defect-related emission at around 3.47 eV.

A heterojunction light emitting device (LED) based on AlNNWs and *p*-type silicon carbide (*p*-SiC) had been demonstrated. When an applied voltage greater than 8 V was applied to the LED, a broad band emission peaked at 417 nm could be observed. The peak deconvolution by Gaussian curve fitting revealed four emission peaks centered at ~400, ~420, ~468, and ~525 nm. These emission peaks were attributed to the nitrogen vacancies (V_N) and O_N trap-levels of the nanowires.

List of Publications

1) Y. Y. Hui, S. P. Lau and X. H. Ji, "Room temperature cathodoluminescence of AlN nanorods," Procceedings. ICMAT 2009, Compound Semiconductor Photonics: Materials, Devices and Integration, Singapore: Pan Stanford Publishing (2010)

2) (H. Y. Yang), (S. F. Yu), Y. Y. Hui and S. P. Lau, "Electroluminescence from AlN nanowires grown on *p*-SiC substrate," Applied Physics Letters, **97** 191105 (2010)

Acknowledgements

The graduate study at The Hong Kong Polytechnic University has been one of the most important and exciting periods in my life. I would like to express my deep appreciation to many people who have favored me with a lot of help and made these years enjoyable and fruitful.

First and foremost, I would like to express my sincerest and deepest appreciation to my supervisor, Prof. S. P. Lau, for his professional and invaluable advices throughout the past two years in my MPhil study. His great broad view, deep insight and enthusiasm towards research have always been a great inspiration to me in defining the most important scientific problems. His opinions helped me through many difficulties in my study and research.

I specially thank Prof. H. X. Jiang, Mr. XiangKe Cao and Mr. A. Sedhain for their help in the PL measurement as well as their great interest and strong support of my work when I attached to Texas Tech University.

Special thanks are also due to Dr. W. Lu for his help in the TEM measurement, Dr. F. K. Lee for the nanoimprinting and AFM operations, Dr. A. Zapien for the SEM and CL measurement and Dr. H. Y. Yang for the measurement of LED. Their supports to my work are highly appreciated.

I have also enjoyed working with an outstanding group of highly motivated people. I would like to thank my research companions: Mr. Vincent Chan, Ms. H. L. Li, Mr. H. F. Wong, Mr. Sherman Mok, Mr. Johnson Wei, Dr. C. Yip and Mr. Simon Luk for their useful suggestions and assistant.

Last but not least, I would like to thank my parents for their patience and endless support throughout my life. They have been inspiring me at every moment.

Table of content

Certificate of Originality i
Abstract ii
List of Publications v
Acknowledgements vi
Table of content viii
List of Figures xi
List of Tables xv
Chapter 1 Introduction 16
1.1 Background 16
1.2 Motivation 18
1.3 Overview 19
Chapter 2 Properties and growth of AlNNWs 22
2.1 Background 22
2.2 Structural and chemical properties 24
2.3 Electrical properties 25
2.4 Optical properties 26
2.5 Magnetic properties 29
2.6 Growth of 1D AlN nanostructures 30
2.6.1 Bottom-up approaches 30
Chapter 3 Experimental details 34
3.1 Experimental setup 34
3.2 Experiment procedures 36

3.3 Structural characterization 37

3.3.1 X-ray diffraction (XRD) 37

3.3.2 Scanning Electron Microscopy (SEM) 39

3.4 Transmission electron microscopy (TEM) 41

3.4.1 Raman spectroscopy 41

3.5 Optical characterization 43

3.5.1 Cathodoluminescence (CL) 43

3.5.2 Photoluminescence (PL) 47

3.6 Magnetic characterization 48

3.6.1 Vibrating sample magnetometer (VSM) 48

Chapter 4 Structural and Magnetic properties 50

4.1 Introduction 50

4.2 Effect of growth temperature 51

4.3 AlNNWs 52

4.3.1 Effect of growth time 52

4.3.2 Structural properties 53

4.4 Zigzag AlNNWs 58

4.4.1 Effect of growth time 58

4.4.2 Structural properties 59

4.4.3 Magnetic properties 65

4.5 Summary 67

Chapter 5 Optical properties 69

5.1 Introduction 69

5.2 AlNNWs 70

5.2.1 Room temperature PL and CL 70

5.2.2 10 K PL 71

5.2.3 Effect of growth time 72

5.2.4 Effect of NH_3 annealing 73

5.3 Zigzag AlNNWs 74

5.3.1 Room temperature PL and CL 74

5.3.2 10 K PL 76

5.3.3 Effect of growth time 77

5.3.4 Effect of NH_3 annealing 78

5.4 Summary 79

Chapter 6 Lighting emitting device (LED) 80

6.1 Introduction 80

6.2 Fabrication 81

6.3 Structural properties 82

6.4 Electrical properties 83

6.5 Optical properties 85

6.6 Summary 90

Chapter 7 Conclusion and Future Work 91

7.1 Conclusion 91

7.2 Future Work 93

References 95

List of Figures

Fig. 2.1 (a) The energy band diagram of Mg-doped AlN thin film. (b) Typical PL spectra of undoped and Mg-doped AlN thin films.[6] ... 27

Fig. 2.2 Schematic illustration of the formation of AlNNWs by catalyst-assisted VLS method.[58] ... 31

Fig. 2.3 Schematic illustration showing the growth process of Si-doped AlN nanoneedles on catalyst-seeded substrate by VLS method.[58] ... 32

Fig. 2.4 Schematic illustration showing the formation process of AlN nanotips by VS process.[58] ... 33

Fig. 3.1 Schematic diagram of the horizontal tube furnace 34

Fig. 3.2 The temperature gradient of the horizontal tube furnace set at 1450 °C. ... 35

Fig. 3.3 Flow chart of the growth process. ... 37

Fig. 3.4 Schematic diagram showing the principle of XRD. ... 38

Fig. 3.5 Schematic diagram showing the principle of SEM. ... 40

Fig. 3.6 Schematic diagram showing the principle of Raman scattering ... 42

Fig. 3.7 The photo of the CL setup. ... 44

Fig. 3.8 The schematic diagram of the CL setup. ... 44

Fig. 3.9 The sensitivity spectrum of the USB 4000 Ocean Optics spectrometer.[70] ... 46

Fig. 3.10 The sensitivity spectrum of the MayaPro2000 Ocean Optics spectrometer.[70] ... 46

Fig. 3.11 Schematic diagram showing the PL system at TTU. ... 48

Fig. 3.12 Schematic diagram showing the setup of VSM ... 49

Fig. 4.1 (a) SEM images of the nanowires prepared at 1450 °C and (b) zigzag nanowires prepared at 1350 °C. 51

Fig. 4.2 (a) SEM images of the nanowires grown on sapphire substrates at 1450 °C with growth time of 1 hr, (b) 2 hr and (c) 3 hr. 52

Fig. 4.3 Comparison of the XRD patterns between nanowires and AlN raw powder. .53

Fig. 4.4 Raman spectrum of the nanowires.. 54

Fig. 4.5 (a) Low and (b) high magnification SEM images of the nanowires. 55

Fig. 4.6 (a) Typical TEM image of a single nanowire. (b) HR-TEM image of the same nanowire showing the crystal lattices. (c) The corresponding SAED pattern. (d) The corresponding EDX pattern obtained by TEM. 57

Fig. 4.7 (a) SEM images of the zigzag nanowires grown on sapphire substrates at 1350 °C with growth time of 1 hr, (b) 2 hr and (c) 3 hr. 58

Fig. 4.8 Comparison of the XRD diffraction patterns between zigzag nanowires and AlN raw powder. 59

Fig. 4.9 Raman spectrum of the zigzag nanowires. 60

Fig. 4.10 (a) Low and (b) high magnification SEM images of the zigzag nanowires grown on sapphire substrate.. 61

Fig. 4.11 (a) Typical TEM image of a single zigzag nanowires. (b) HR-TEM image of the same zigzag nanowire showing the crystal lattices. (c) The corresponding SAED pattern. (d) The corresponding EDX pattern. 62

Fig. 4.12 (a) Typical TEM image of a single zigzag nanowires showing the relationship between the turning angles and the surfaces. (b) A structural model of wurtzite h-AlN and the corresponding crystal planes. (c) Schematic diagram showing the growth process of zigzag nanowires.[76] 63

Fig. 4.13 (a) HR-TEM image of a single zigzag nanowire. The inset shows the corresponding electron diffraction pattern. To the right shows the enlarged image of the marked area. (b) Schematic diagram showing the formation of an extra half plane. 65

Fig. 4.14 *M-H* loop of the zigzag nanowires grown on sapphire with growth time 2 hr measured at room temperature and applied field parallel and perpendicular to the sample surface. 66

Fig. 5.1 (a) PL spectra and (b) CL spectra of the nanowires grown on sapphire substrate and alumina tube. 70

Fig. 5.2 The comparison between the room temperature PL and 10 K PL spectra of the nanowires. The inset shows the magnified image of the 10 K PL spectrum from 5.7 eV to 6.2 eV. 71

Fig. 5.3 (a) Room temperature PL and (b) CL spectra of the nanowires with growth time of 2 hr and 3 hr. 72

Fig. 5.4 (a) PL spectra of the nanowires synthesized at 1450 °C with growth time of 2 hr and 3 hr. (b) PL spectra of the corresponding nanowires annealed at 900 °C under the flow of ammonia (NH_3) gas for 2 hr. 73

Fig. 5.5 (a) The PL and (b) CL spectra of the zigzag nanowires grown on sapphire substrate 74

Fig. 5.6 Room temperature PL and 10 K PL spectra of the zigzag nanowires. The inset shows the magnified image of the 10 K PL spectrum from 4.62 eV to 5 eV. . 76

Fig. 5.7 (a) Room temperature PL spectra and (b) CL spectra of the zigzag nanowires synthesized at 1350 °C with growth time of 2 hr and 3 hr. 77

Fig. 5.8 (a) PL spectra of the zigzag nanowires synthesized at 1350 ^{o}C with different growth time of 2 hr and 3 hr. (b) PL spectra of the annealed zigzag nanowires synthesized at 900 ^{o}C under the flow of NH_3 gas for 2 hr. 78

Fig. 6.1 Schematic diagram showing the heterojunction LED. 81

Fig. 6.2 (a) A typical SEM image of the randomly packed nanowires. (b) A magnified SEM image of a single nanowire. (c) Cross-section SEM image of the interface between nanowires and *p*-SiC substrate. (d) HR-TEM image of a single nanowire and the inset shows the corresponding SAED pattern. 82

Fig. 6.3 (a) Room-temperature *I-V* characteristics of the heterojunction LED. The inset shows the schematic diagram of the proposed heterojunction LED. (b) Room-temperature *I-V* curves of two ITO contacts deposited on a layer of randomly packed nanowires. The inset shows the corresponding measurement setup. 84

Fig. 6.4 Room-temperature EL spectra of the heterojunction LED under bias voltages of 8 V, 9.6 V, 11.2 V and 14.6 V. 85

Fig. 6.5 EL spectrum with the fitting results of the LED under forward biased voltage of 14.6 V. The inset shows the sum of the four Gaussian peaks. (b) PL spectrum with the fitting results of the nanowires deposited on the *p*-SiC substrate. 87

Fig. 6.6 Energy band diagrams for the heterojunction under forward bias and at equilibrium. E_{Def} represents the four trap-level states of the nanowires. 88

Fig. 7.1 Schematic diagram of the new horizontal tube furnace setup. 93

List of Tables

Table. 4.1 Comparison between nanowires and zigzag nanowires. 67

Chapter 1 Introduction

1.1 Background

Aluminum nitride (AlN) is an important member of the group III nitrides, with the highest bandgap of about 6.0 eV. The common crystal structure of AlN is a wurtzite hexagonal structure (h-AlN), which consists of two interpenetrating hexagonal closely-packed sublattices, each with one type of atom either Al or N. AlN exhibits excellent thermal conductivity, good electrical resistance, low dielectric loss, high piezoelectric response and thermal expansion coefficient matching silicon,[1] giving it strong potential for deep ultraviolet optoelectronic applications.

To date, different active devices have been based on low bandgap semiconductor materials, such as silicon and indium phosphide. Wide bandgap materials, such as gallium nitride (GaN), is also one of the attractive candidates for short wavelength optoelectronic devices and high-power and high-temperature electronics.[2] Compared to GaN, AlN has a wider band-gap that makes it a promising material for optoelectronic applications in deep UV range. Due to this reason, many researches on fabricating AlN based devices are ongoing. Recently, different AlN-based devices have been demonstrated using AlN thin films. For examples, ~210 nm deep ultraviolet *p-n* junction diode;[3] ~202 nm deep UV photodetector;[4] and combustible gas sensor have been demonstrated by various research groups.[5]

Although AlN has a lot of potential in the development of optoelectronic devices as mentioned above, it is essential to obtain device quality materials. Thus, it is desirable to

obtain conductive *n* and *p*-type AlN. However, it is very difficult to enhance the conductivity of AlN due to the large activation energy of dopants and the simultaneous generation of compensating centers and defects during the crystal growth.[6] Recently, many reports have successfully illustrated *n* and *p*-type doping of AlN thin films, such as Si-doped AlN films[7,8] and Mg-doped AlN films respectively.[6]

Apart from semiconductor thin films, semiconductor nanowires have demonstrated significant potential as fundamental building blocks for nanoelectronics and nanophotonic devices. Many reports have illustrated the superior and unique properties of semiconductor nanowires that outrun the traditional thin film technologies.[9] Some of the appealing features of nanowires are that they can be single-crystalline,[10] relatively defect-free,[11] having high surface to volume ratio, having atomically smooth surfaces and able to accommodate large lattice mismatch with substrate.[12] These special features allow the development of novel devices, such as single nanowire field-effect transistor (FET) with faster processing speed,[13] and nanosensor with higher sensitive.[14] In that case, the abilities to synthesize single crystalline nanowires with precisely controlled and tunable chemical composition, size, structure and morphology and to dope them with both *p* and *n*-type dopants have opened up opportunities for assembling almost any kind of functional nanosystems ranging from photonics and electronics to biological sensors.[15]

Nanophotonoics devices such as light-emitting diodes (LEDs),[16] waveguides, electrically driven single nanowire lasers,[17] and photodetector,[18] have all been successfully demonstrated in low bandgap semiconducting nanowires. There are no

reports on AlN nanowires (AlNNWs) based optoelectronic devices up till now because the doping of AlNNWs is scarce despite the successful demonstration of high-crystal quality AlNNWs. Therefore, it is of significant technological interest to study the doping of AlNNWs.

1.2 Motivation

Compact high-efficiency ultraviolet solid-state optoelectronic devices, such as LEDs and laser diodes (LDs) are of considerable technological interest as alternatives to large, toxic, low-efficiency gas lasers and mercury lamps. Microelectronic fabrication technologies and the environmental sciences both require light sources with shorter emission wavelengths: the former for improving resolution in photolithography and the latter for allowing sensors to detect minute hazardous particles. In addition, ultraviolet solid-state optoelectronic devices also draw attentions for potential applications in high-density optical data storage, biomedical research and water and air purification. AlN is one of the potential materials for deep ultraviolet LEDs and laser diodes but it is suffering from difficulties in controlling electrical conduction and large lattice mismatch with substrates in thin film technology.[3]

It has been reported that the use of semiconductor nanowires can significantly enhance the performance of different optoelectronic devices such as transistors, solar cells, LEDs and so on.[19] The utilization of more effective ultraviolet solid-state devices based on AlNNWs can further improve the device performance. Since the *n* and *p*-type doping in AlNNWs have not been demonstrated, it is essential to investigate the *n* and *p*-type doping in AlNNWs so as to increase the carrier concentration and mobility, which makes

it possible for optoelectronic applications.[20] Although there are different dopants that can successfully dope into AlNNWs such as Si, Fe, Cu, Mn and Co,[21-24] no reports so far can show the *n* and *p*-type conduction in AlNNWs.

This project aims at fabricating single-crystalline Mg-doped AlNNWs. The nanowires have been grown on different substrates such as sapphire, silicon carbide (SiC) and alumina. It is known that Mg is a potential *p*-type dopant in AlN.[25] Therefore, the structural and optical properties of the doped nanowires as a function of growth parameters have been investigated systematically in order to determine the role of the Mg inside the AlN. Mg-doped AlNNWs with different surface morphologies, growth times and growth temperatures were synthesized. These parameters are correlated with their optical properties so that the optimized growth conditions for the nanowires can be obtained. In order to demonstrate that AlNNWs are competent to optoelectronic applications, an AlNNWs-based LED has been synthesized to illustrate the possibility of fabricating AlNNWs-based optoelectronic devices.

1.3 Overview

The objective of this project is to fabricate Mg-doped AlNNWs under different conditions so as to study the correlation between the growth conditions and optical and structural properties. By understanding their optical properties, the fabrication of Mg-doped AlNNWs based optoelectronic devices such as LED would be possible.

In chapter 1, the background and advantages of AlN are introduced. Some problems of applying AlN in optoelectronic devices are discussed. The objective of this project together with the motivation is also included.

In chapter 2, brief information of the AlNNWs is introduced. The unique structural, chemical, optical, electrical and magnetic properties of AlNNWs are described. Also, the growth methods of AlNNWs have been included in this chapter.

In chapter 3, the experimental details are described, including the techniques for the optical and structural characterizations, such as X-ray diffraction (XRD), Raman spectroscopy, scanning electron microscopy (SEM), transmitting microscopy (TEM), vibrating sample magnetometer (VSM), cathodoluminescence (CL) and photoluminescence (PL). The experimental setup and procedures for the growth of AlNNWs are described.

In chapter 4, the structural properties of AlNNWs and zigzag AlNNWs as a function of growth conditions are studied. The effects of Mg dopant on the magnetic properties of the AlNNWs and zigzag AlNNWs are discussed.

In chapter 5, the optical properties of AlNNWs and zigzag AlNNWs are studied as a function of oxygen concentration. The effects of Mg dopant on the optical properties of the nanowires are also investigated.

In chapter 6, a heterojunction LED based on AlNNWs and *p*-type (4H) silicon carbide (*p*-SiC) has been demonstrated. It illustrates the potential application of AlNNWs into optoelectronic devices.

In chapter 7, the important findings on AlNNWs are concluded and the future work is discussed.

.

Chapter 2 Properties and growth of AlNNWs

2.1 Background

The requirement for more powerful and compact systems in electronic and optical devices have been growing, there are new branches of material researches in the development of nanoscale devices in order to make the devices smaller. Semiconductor nanostructures have emerged as a powerful class of materials that are creating substantial opportunities for nanoscale photonic and electronic devices.[26] For example, the nanoscale materials can exhibit size-dependent emission or excitation,[27] quantized conductance,[28] Coulomb blockade or single-electron tunneling[29] and metal-insulator transition.[30] These phenomena predict a deep insight to control the optical, electrical, magnetic and thermoelectric properties of functional materials. Particularly in nanowires, they have some appealing advantages over the other systems as they can remain their transport capabilities while maximizing their quantum confinement effects. Numerous of nano-devices with outstanding properties based on nanowires have already been demonstrated, such as field effect transistor (FETs),[31] inverters, bipolar transistors,[32] light emitting diodes (LED)[33] and logic gates.[34]

Researches on the properties and growth of one dimensional (1D) AlN nanostructures have been widely investigated due to their superb properties. AlN nanostructures such as nanowires, nanobelts and nanotubes were found to possess promising applications in photonic devices. Although AlNNWs permit numerous applications, control of the large concentration of impurities in this wide-band gap semiconductor is still a big challenge. To date, most of the studies still concentrate on the optical properties of AlNNWs due

to the inability to obtain near bandedge emissions and to eliminate oxygen impurities. The crucial information regarding transport properties of carriers are rarely investigated because the highly insulating nature of AlN particularly hampers the electrical characterization of AlNNWs.[35]

However, various reports on the electrical behaviors of AlNNWs have been successfully illustrated recently, which are giving strong proof on the semiconducting behavior of AlNNWs and its capability to apply in optoelectronic applications. For examples, the electrical properties of a single AlNNW have been reported. The resistivity of the nanowire was measured to be 10^6 Ωcm.[36] Moreover, the photoconductivity in a single AlNNW has also been demonstrated. Photocurrent responses were detected when the nanowire was illuminated by a laser with wavelength close to its bandgap.[6] Because the resistivities of the AlNNWs are still high, it is necessary to obtain conductive AlNNWs.

It is believed that the optical and electrical properties of AlNNWs can be improved by doping different dopants into AlNNWs and different devices can be fabricated using the doped nanowires as the building blocks. Particularly, the low hole mobility in AlN can be improved by introducing *p*-type dopants, which would allow the fabrication of deep UV light emitting devices. Therefore, it is of importance to illustrate *p*-type doping in AlNNWs, such as Mg-doped AlNNWs so that optoelectronic devices can be fabricated.[37]

2.2 Structural and chemical properties

AlN is a compound of aluminium and nitrogen exhibiting wurtzite hexagonal (h-AlN) structure with molecular weight of 40.99 g/mol. This material is stable at high temperatures in inert atmospheres and melts at 2200 ^{o}C. In vacuum ambient, AlN decomposes at ~1800 ^{o}C. AlN was first reported to have the wurtzite hexagonal crystal structure with lattice constants a = 3.11 Å and c = 4.98 Å.[38] Jeffrey and Parry[39] suggested that the AlN lattice varied slightly from the ideal wurtzite structure. The presently accepted values for the AlN lattice constants quoted in the literature are a = 4.982 Å and c = 3.112 Å.[40] The lattice constants can be changed if oxygen contamination is found.[41]

It is well known that the mechanical properties of a solid, such as Young's modulus, yield strength, plastic deformation and failure, are determined by the material size, density of dislocations, interface-to-volume ratio and grain size. These factors can dramatically affect the hardness and yield strength of a material. For the AlNNWs, dislocation and defect free, and relatively smooth surface can be produced so that these problems can be omitted and the physical properties of the solid can be enhanced. For example, it is found that the AlN nanowires can have better elastic properties when compared with bulk AlN. This value decreases when the diameter of the nanowire increases since the behavior of the nanowire tends towards that of the bulk.[42]

Moreover, the lattice constants of AlN can be changed easily in nanowires. According to a well accepted vapor–liquid–solid (VLS) growth mechanism for 1D nanomaterials, the anisotropic crystal growth of wurtzite AlN is promoted by the presence of liquid

alloy and solid interface.[41] It is conceivable that the size and diameter of the as-synthesized products can be controlled by selecting catalysts with different sizes. The other growth mechanism of AlNNWs is vapor–solid (VS) growth process.[43] Yazdi et al. have demonstrated that a defect-free and smooth surface of AlNNWs with single crystalline hexagonal structure can be produced by VS growth process[44] and Shi et al.[45] have demonstrated dislocation-free AlN nanotips using VS process.

The physical structure of the Mg-doped AlNNWs is expected to have the wurtzite h-AlN structure. It is believed that the Al site will be substituted by Mg as they are having similar atomic sizes. Moreover, the lattice constant of the doped nanowires should be larger than the undoped ones because the atomic size of Mg is 1.45 Å, which is larger than that of Al (1.18 Å).[25]

2.3 Electrical properties

It is difficult to measure the resistivity of AlN thin films due to its low intrinsic carrier concentration, deep native defect and impurity energy levels. Edwards and co-workers calculated the resistivity of a single crystalline AlN to be 10^{11} to 10^{13} Ωcm.[43,46] It is believed that the resistivity of AlNNWs can be much lower than the resistivity of bulk AlN due to the smaller effective mass for holes and electrons attributed by the confinement effect. Also, the carrier concentration of AlN can be improved by doping *n* or *p*-type dopants into the AlN lattice. For example, at room temperature, Jiang's group have measured the resistivity of the Mg-doped AlN thin film to be about 10^7 Ωcm.[6] Although the resistivity is still too large to be useful in device applications, after optimization of the film, the resistivity is about 450 Ωcm when it is measured at 850 K.

The conduction at high temperature is due to the hole activation from Mg acceptors. This is because at high temperature, the Mg dopants can be activated by breaking the Mg bondings with defects, which are incorporated into the as-grown samples intrinsically.[7,47]

On the other hand, Zheng's group has calculated the resistivity of a single AlNNW, which has a resistivity of 10^6 Ωcm.[36] It is found that different 1D AlN nanostructures have the same order of resistivity.[43,46] The temperature dependent *I-V* characteristics have also demonstrated in that report, which gives strong proof on the semiconductor properties of AlNNWs.

2.4 Optical properties

A band-edge emission centered at ~6.0 eV from undoped AlN thin film has been found from various reports due to the recombination of free excitons and exhibits virtually no impurity transitions in low energy region.[48] Although the bandgap of AlN is ~6.0 eV, many groups have observed broad emission peaks below 6.0 eV,[49] which are believed to be due to oxygen contaminations mostly. It is found that the concentration of oxygen can change the position of the defect peak from 3.3 to 4.0 eV.[45] It is also suggested that the nitrogen vacancies and Al interstitial point defects are responsible for the 2.1 eV emission band.[50] It is also observed a broad emission ranging from 2-3 eV with a peak centered at 2.8 eV.[51]

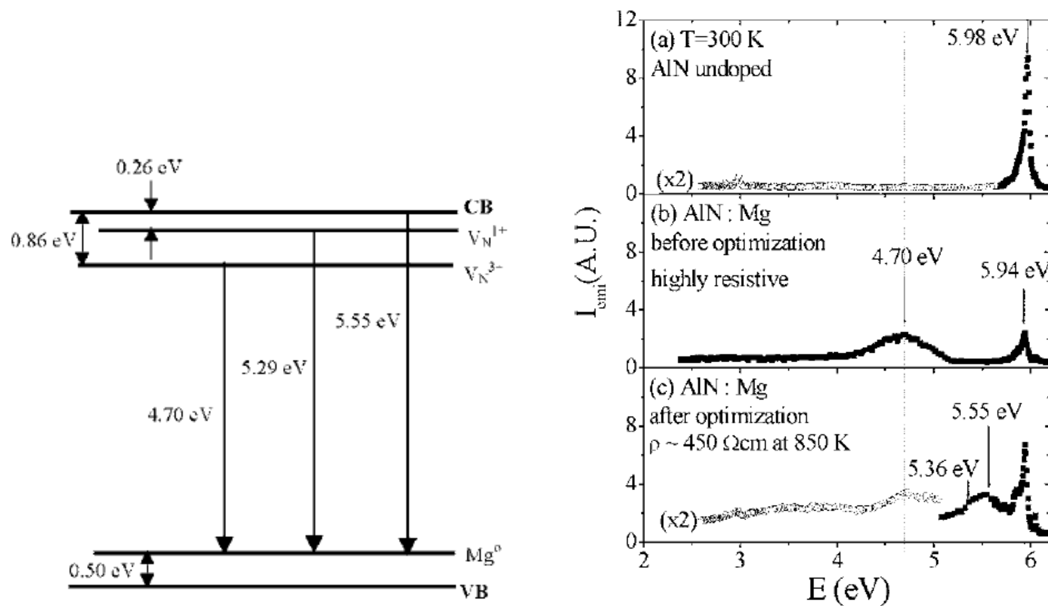

Fig. 2.1 (a) The energy band diagram of Mg-doped AlN thin film. (b) Typical PL spectra of undoped and Mg-doped AlN thin films.[6]

The optical transitions of undoped and Mg-doped AlN thin films can be described by the energy band diagram as shown in Fig. 2.1(a). It is believed that the energy states from oxygen-free Mg-doped AlN thin film should only consist of nitrogen vacancies and Mg acceptors in the energy band of AlN. It is found that the intensity of the near bandedge emission centered at 5.94 eV can be enhanced after the optimization of the thin films. Moreover, two more extra emissions centered at 5.36 eV and 5.55 eV are detected whereas the emission center at 4.7 eV is suppressed. As shown from Fig. 2.1 (b), all the emissions are attributed to the deep level Mg acceptor state, except the emission from the near band centered at 5.94 eV. Therefore, by similar approach, the bandgap of AlNNWs could also be minimized by doping Mg and transform it into possible *p*-type AlNNWs.[52]

As mentioned above, due to the native ability of AlN to form surface oxide layers of 5-10 nm even at room temperature, it is believed that the oxidation of the AlNNWs surface are

very severe and difficult to eliminate. As a result, most reports cannot obtain the near band emissions from the AlNNWs due to the oxygen related trapped levels between the conduction band and valence band of AlN.[53] So far, to our knowledge, only three literatures can successfully detect the near bandedge emissions from AlNNWs, which is the 209 nm emission from Yazdi et al.,[44] the 204 nm emission from Shi et al.,[45] and the 212 nm emission from Ji et al.[24] In addition, it is demonstrated that the intensity of the near bandedge emission peak from the AlN nanorods could be enhanced significantly by introducing Fe dopant.[21] The energy confinement in nanowires may play an important role in this phenomenon as the strength of optical transition is directly related to the density of states and is dramatically enhanced for quantum wire structure. Also, the exciton binding energy in quantum wire is significantly enhanced.

As calculated theoretically, the confinement effect gives a lot of advantages in AlNNWs. Firstly, there should be a strong quantum confinement in AlNNWs morphology and increase in the energy bandgap with respect to the diameters of the nanowires. This is because the spatial distribution of free carriers or excited electron-hole pairs in nanostructures is confined within a relatively small volume when the physical length of the nanostructure becomes small enough. Hence, the gain of the electro-optical signals and the distinctively non-linear optical properties can be enhanced dramatically. Indeed, a systematic blueshift of the optical emission corresponding to the size reduction of the other materials has already been demonstrated.[54] Yet, there are still no reports on the confinement effect on AlNNWs.

Secondly, the growth methods and conditions can significantly affect the optical properties of the AlNNWs in terms of emission intensity and position, spectral shape, and the existence of long wavelength components from impurity or defect states.[21,55,56]

Thirdly, nanowires are able to function as effective optical waveguides because of their tight photon confinement in sub-wavelength size, which is induced by the huge dielectric mismatch between the material and its surrounding environment. In other words, if a nanowire is being excited by photon, the emission from its ends can be enhanced.

2.5 Magnetic properties

Diluted magnetic semiconductors (DMSs) are attractive materials for spintronics, which combines the inherent properties of both semiconductor and ferromagnetic materials. It can be done by doping transition metals into AlN. The AlNNWs based DMSs have been reported by many groups, such as Fe-doped AlN nanorods,[21] Cu-doped AlN nanorods,[24] Mn-doped AlNNWs[22] and Co-doped AlN nanorods.[23]

It is proven that ferromagnetism at or above room temperature can be observed from AlN by doping different kinds of transition metals.[57] For example, a simulation result from Wu et al. have predicted the capability of making AlN into DMS by doping Mg.[25] When the Mg dopant in AlN substitutes the Al vacancy, it will lead to spin-polarized ground states by forming MgN_4 tetrahedral structures. It is predicted that the ferromagnetism can occur in AlN doped with 7% of Mg at the growth temperature of 2000 K under N-rich condition.[25] This result gives a very good prospect for the ferromagnetic properties of Mg-doped AlNNWs.

2.6 Growth of 1D AlN nanostructures

2.6.1 Bottom-up approaches

The essence of 1D nanostructure formation is crystallization which involves two fundamental steps: nucleation and growth. There are three types of bottom-up approaches to achieve the growth of 1D AlN nanostructures, which are (i) catalyst-assisted VLS process, (ii) catalyst-free VS process and (iii) template-confined synthesis.[58] The advantages of bottom-up growth processes are enhanced radiative recombination efficiency and virtually substrate dislocation free.

(i) Catalyst-assisted VLS process

The nucleation of a typical vapor liquid solid (VLS) process are mainly induced and dictated by catalyst liquid droplets. Without using catalyst, the growth mechanism of the single-crystalline nanostructures should be a self-catalyst VLS process. For the catalyst-assisted VLS process, where the original idea goes back to the 1960s,[59] the catalyst plays an important role for the crystal growth because it induces the formation of liquid alloy droplets with the vaporized reactants and serves as a seed for the nucleation of the nanowires on a substrate at lower temperature zone. It is crucial that the catalyst has to be chosen such that it can form eutectic alloy with the reactant material and hence the liquid droplets can be formed. Therefore, this method is restricted by the choice of catalyst and reactant material. Recently, there are some reports about growing 1D AlN nanostructures (nanofibers, nanowires, nanotips, etc.) by using different catalysts.[60] For example, Shi and co-workers demonstrated that uniform AlN nanotips were synthesized with Au catalyst layer of different thickness. In their experiment, the size control of the nanotips was achieved simply by adjusting the

thickness of the gold layer and keeping the other growth parameters unchanged.[60] The growth mechanism is shown in Fig. 2.2. The advantage of this method is that the nanowires can be patterned in the way of the seed layer pattern.

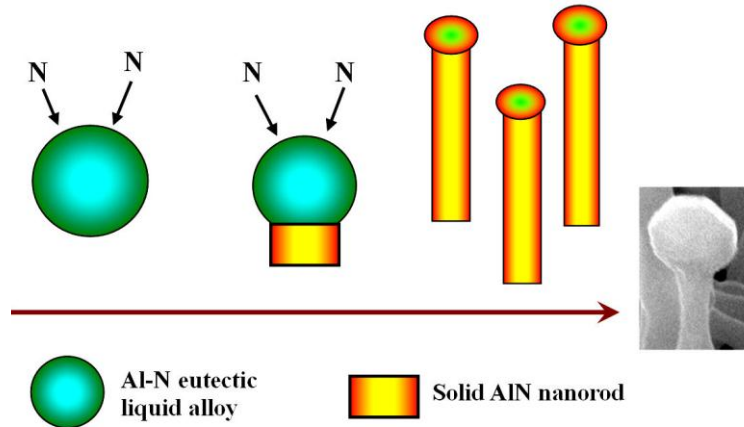

Fig. 2.2 Schematic illustration of the formation of AlNNWs by catalyst-assisted VLS method.[58]

Moreover, by preparing catalyst-seeded substrate, the metal catalyst can be doped into the AlN nanostructure if the catalyst is chosen carefully. From Tang and his co-workers, Si-doped AlN nanoneedles were synthesized by preparing a patterned Co seed layer on top of Si substrate. The growth mechanism can be described by Fig. 2.3.[61] The disadvantage of catalyst-assisted VLS is that the catalyst for growing the nanowires is always irremovable. This can affect the purity of the nanowires, which results in the deterioration of optical property and the crystallinity of the nanowires.

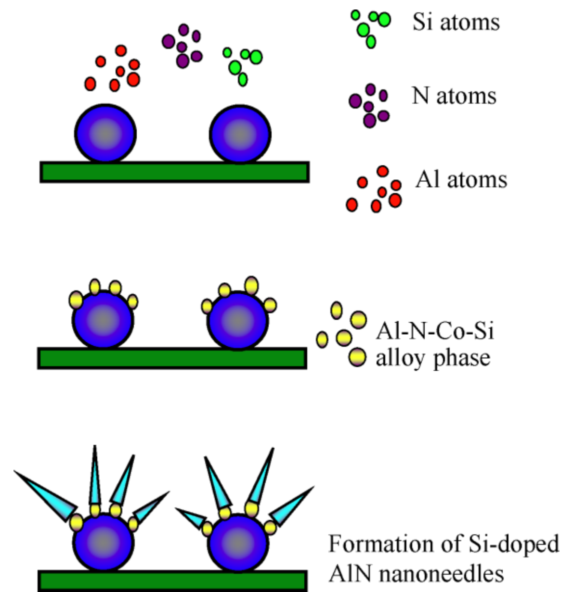

Fig. 2.3 Schematic illustration showing the growth process of Si-doped AlN nanoneedles on catalyst-seeded substrate by VLS method.[58]

(ii) Catalyst-free VS process

VS growth has been proven to be an effective catalyst-free method for synthesizing 1D nanostructures. The key feature shared by the VS process is the existence of large difference in growth rate along different crystal orientations. The occurrence of highly anisotropic growth can be inherent in the wurtzite III-V system, which offers an opportunity for forming 1D nanostructures in a wide range of conditions. Although the exact mechanism of this approach is still not clear, it has been used by many research groups to synthesize nanowires. The major advantage of this method is its simplicity and accessibility. In a typical process, the vapor species is first generated by evaporation, chemical reduction and other gaseous reactions. These species are subsequently transported and condensed onto the surface of a solid substrate placed in a tube furnace with temperature lower than that of the source material. With proper control over the supersaturation factor, large scale 1D nanostructures can be achieved.[58]

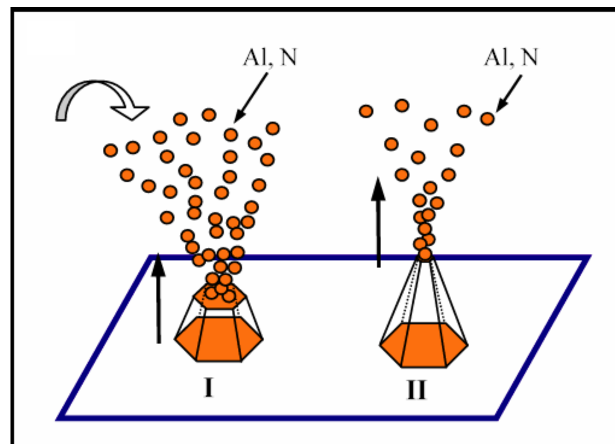

Fig. 2.4 Schematic illustration showing the formation process of AlN nanotips by VS process.[58]

(iii) Template assisted growth method

The template-based techniques have been widely applied to produce nanowires. In this method, templates, such as carbon nanotubes (CNTs) and anodic alumina membrane, provide confined spaces in a nanometer scale for the formation of nanowires.[58] Template-based synthesis provides a simple and direct route to greatly expand the diversity of materials that can be processed as uniform nanowires with controllable size. However, when a template is utilized, it is often necessary to isolate the template using post-treatment to obtain the desired nanowires, and the removal of the template is often difficult and tedious. Furthermore, one of the major problems is that the nanowires synthesized using this method is often polycrystalline in structure, and the quantity that can be produced is relatively limited. For example, Wu et al. have synthesized aligned AlNNWs by a direct reaction of metal Al vapor with flowing ammonia gas under the confinement of anodic porous alumina template.[62]

Chapter 3 Experimental details

3.1 Experimental setup

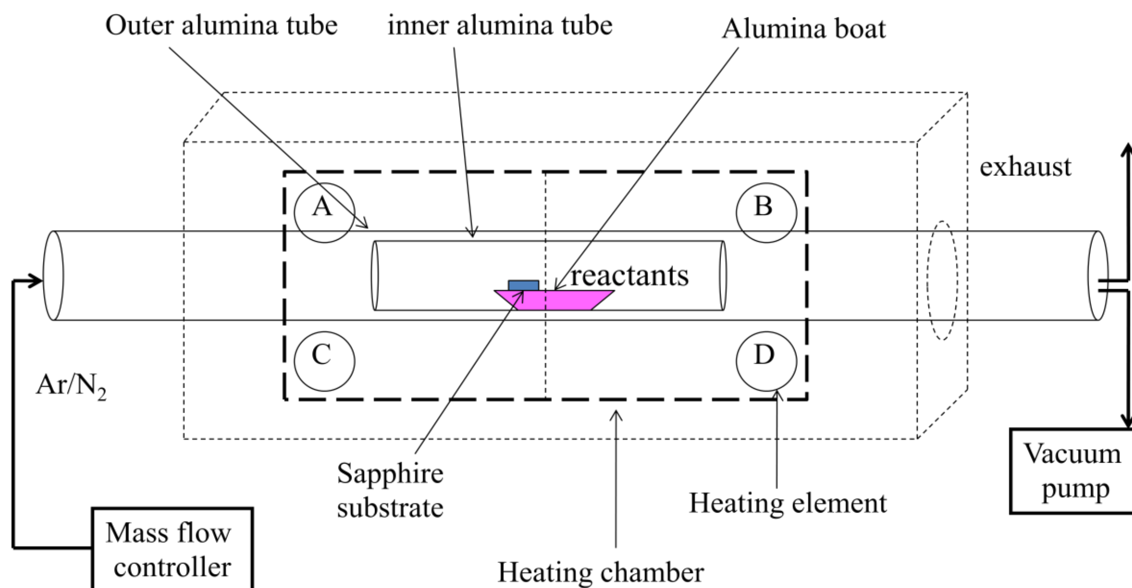

Fig. 3.1 Schematic diagram of the horizontal tube furnace .

A Carbolite single zone tube furnace (model number STF 15/50/180) was used to grow AlNNWs. It consists of four silicon carbide heating elements that arranged symmetrically around a separated alumina tube to ensure excellent thermal uniformity as shown in Fig. 3.1. Circles A, B, C and D indicate the locations of the heating elements in the furnace. The dashed line represents the central position of the furnace which is the highest temperature zone. The maximum temperature of this furnace is 1500 ^{o}C and the length of the heating zone is about 18 cm. The maximum heating rate is about 20 ^{o}C/min for the target temperature below 1200 ^{o}C. For the temperature above 1200 ^{o}C, the maximum heating rate is about 3 ^{o}C/min. It uses independent digital temperature controller to modulate the temperature at the set value.

Inside the tube furnace, it consists of an outer alumina tube (diameter = 4 cm and length = 120 cm), which supply the argon (Ar) and nitrogen (N_2) gases. Inside the alumina tube, there is a small alumina tube (diameter = 3 cm and length = 15 cm), which contains an alumina boat (height = width = 2 cm and length = 8 cm). The reactants can be loaded inside the alumina boat and a substrate was placed on top of the alumina boat facing downward. The whole setup can be pumped into vacuum with both end sealed so as to removed the moisture and air inside the tube furnace.

Since the substrate temperature is critical for the growth of nanowires, the temperature gradient of the tube from the centre of the heating zone was measured by an S-type thermocouple. Figure 3.2 shows the temperature gradient of the tube furnace where the furnace was set at 1450 ℃. It is found that the temperature inside the tube drops almost 50% when the thermocouple was 10 cm away from the centre of the heating zone.

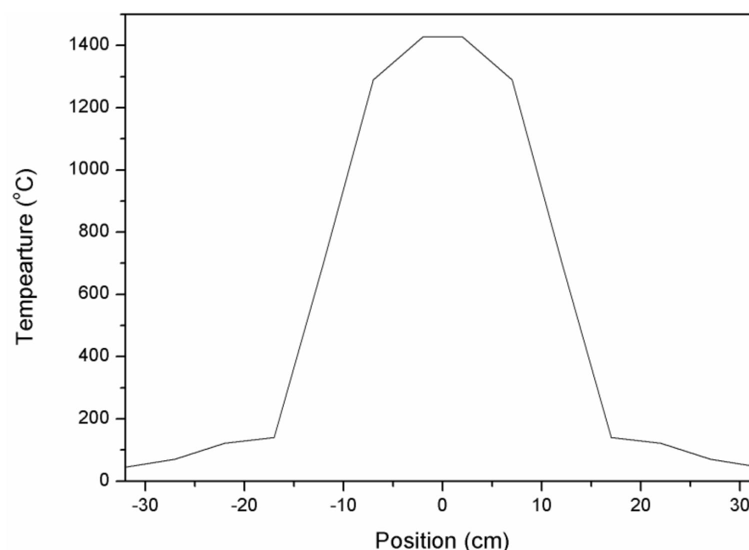

Fig. 3.2 The temperature gradient of the horizontal tube furnace set at 1450 ℃.

3.2 Experiment procedures

AlNNWs were synthesized by a conventional chemical vapor deposition method (CVD). The experiment was carried out inside a horizontal tube furnace by reacting aluminum nitride (AlN, Sigma-Aldrich, 99%) powder, magnesium chloride ($MgCl_2$, Sigma-Aldrich, 99%) powder and nitrogen gas (N_2, 99.995%) together and form nanowires on a substrate at elevated temperature.

For nanowires grown on inner alumina tubes, an inner alumina tube was eroded with NaOH (1 mol) inside a typical tube furnace at 500 ^{o}C for 5 min. It is believed that the defect sites on the eroded alumina tube can initiate the growth and enhance the yield of the nanowires

For the nanowires grown on sapphire substrates, a sapphire (0001) substrate with size of 2 cm by 0.5 cm was pre-cleaned with acetone and isopropyl alcohol (IPA) in an ultrasonic bath for 15 min, respectively. The polished surface of the pre-cleaned substrate was placed facing downward on an alumina boat (facing the reactant powders with a distance of 2 cm). The alumina boat was transferred into the inner alumina tube. Then the inner alumina tube was pushed into the center of an outer alumina tube in the way that the reactants were located at the hottest zone of the furnace.

For both growth processes, 0.5 g of physically mixed AlN and $MgCl_2$ powders in a mass ratio of 2:1 were loaded into an alumina boat. The procedures of the growth process represented by a flow chart are shown in Fig. 3.3. After evacuation of the outer alumina tube to ~10^{-1} Pa for 30 min, Ar gas was introduced into the outer alumina tube to

remove the residual oxygen and moisture before the furnace was turned on. When the pressure of the tube returned to atmosphere pressure, Ar gas of 70 sccm was introduced into the setup and the furnace was then turned on. The setup was first heated with an initial heating rate of 5 °C/min. When the temperature of the setup reached 800 ℃, N_2 gas was introduced into the setup at a flow rate of 70 sccm. The flow rate of N_2 gas was further increased to 140 sccm when the temperature of the furnace reached 1200 ℃. The growth was maintained for 1, 2 and 3 hr at 1350 °C and 1450 ℃ before the furnace was turned off and cooled down naturally.

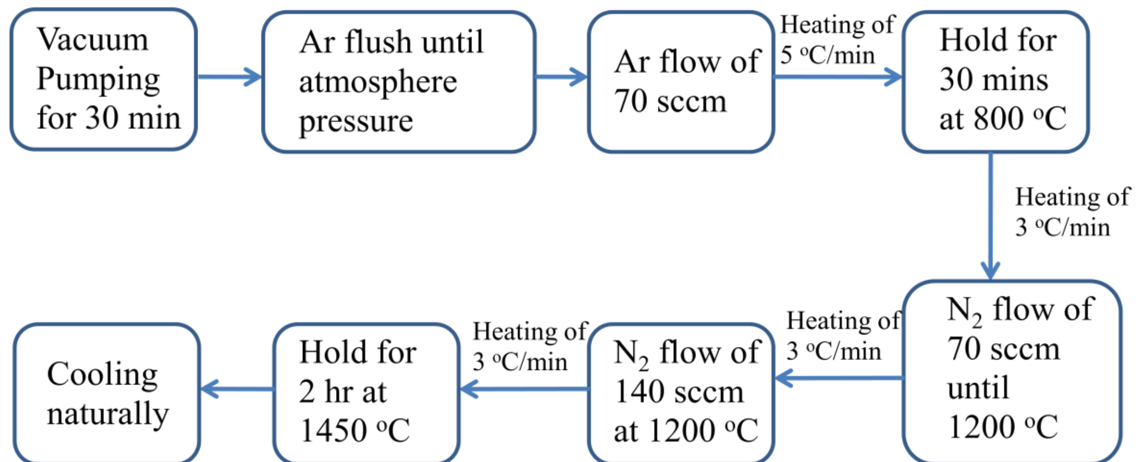

Fig. 3.3 Flow chart of the growth process.

3.3 Structural characterization

3.3.1 X-ray diffraction (XRD)

X-ray diffraction (XRD) is a method to determine the arrangement of atoms within a crystal, which can be either single crystalline or polycrystalline structure. It works when an X-ray beam strikes into a crystal and diffracts into many specific directions, see Fig. 3.4. From the angles and intensities of these diffracted beams, a crystallographer of a certain material can be produced in a three-dimensional (3D) picture by reconstructing each unit cell within the crystal. From the XRD, the positions of the atoms in the crystal,

chemical bonding and disordering can be determined. Another advantage of this method is that it is a non-destructive technique which reveals information regarding unit cell dimension, crystalline structure and phase identification of materials precisely. The structural properties of the nanowires were characterized by a Bruker D8 Discover and a Philip X'pert X-ray Diffractometer in a four-circle mode. The X-ray source gives out K_α radiation of copper (Cu) at wavelength of 1.54 Å .[63]

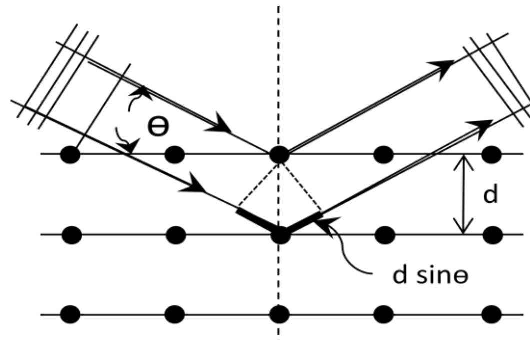

Fig. 3.4 Schematic diagram showing the principle of XRD.

The XRD works when there is a parallel monochromatic X-ray beam hitting on a sample, part of the beam will be diffracted by different crystal planes of the sample. The diffracted rays will interfere with each other to form diffraction centers and form constructive interferences in certain angles. These constructive diffraction interferences of the sample should obey the Bragg's Law:

$$2d_{hkl}\sin\theta = n\lambda$$

(Eq. 3.1)

where d_{hkl} is the inter-planar spacing, n is an integer which represents the number of diffraction mode, θ is the angle of diffracted beam, λ is the wavelength of the incident X-ray beam. For a material with a cubic structure, the inter-planar spacing can de deduced from this equation:

$$d_{hkl} = \frac{a}{\sqrt{h^2 + k^2 + l^2}}$$

(Eq. 3.2)

where h, k and l are the Miller indices.

But for hexagonal structure, the formula should be the following:

$$\frac{1}{d_{hkl}} = \sqrt{\frac{4}{3}\left(\frac{h^2 + k^2 + l^2}{a^2}\right) + \frac{l^2}{c^2}}$$

(Eq. 3.3)

where h, k and l are the Miller indices.

Two different scanning modes, θ-2θ mode and rocking mode, were used to characterize the crystal structure of the AlNNWs. The first mode is to identify the crystalline phases and orientation of the film. In this mode, the X-ray source is fixed, where the sample holder is moving in the speed of ω and the detector is moving in the speed 2ω. The second mode is the crystalline structure measurement of the sample by determining the full width half maximum (FWHM) from the rocking peak. In this mode, The X-ray source and detector are fixed at a selected angle, where the sample holder is rocked back and forth in a few degrees about the θ direction so as to obtain the crystallinity of the sample from the full width half maximum (FWHM) in the rocking curve.[64]

3.3.2 Scanning electron microscopy (SEM)

Scanning electron microscopy (SEM) is a high resolution electron microscope that is able to image the sample surface at a relatively larger area by scanning it with high-energy beam of electrons that generated from an electron gun. The sample's surface topography,

composition and other properties such as electrical conductivity can be obtained when the electrons from the electron gun interact with the atoms from the sample, which is shown in Fig. 3.6.[65]

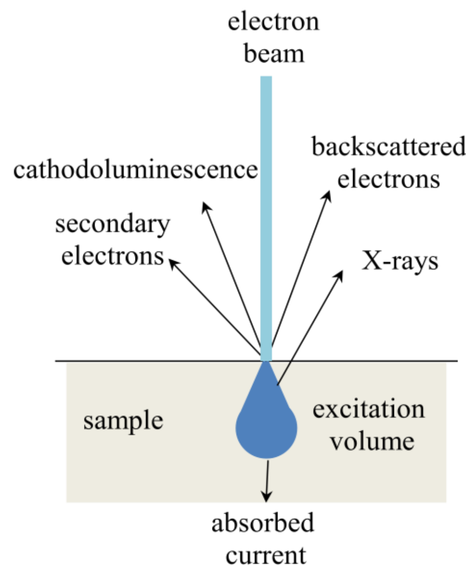

Fig. 3.5 Schematic diagram showing the principle of SEM.

Typically, there are several types of signals produced by SEM, including secondary electrons (SE), back-scattered electrons (BSE), cathodoluminescence (CL), characteristic X-rays, specimen current and transmitted electrons, which are shown in Fig. 3.5. Since AlN is a semiconductor that can conduct electricity, gold coating of the samples is not necessary. Yet, higher resolution image can be obtained if gold is coated onto the samples to reduce the localized charge up on the sample surface. All the samples were characterized by JSM-6335F Field Emission Scanning Electron Microscope by sticking them onto a conducting carbon tape.

3.4 Transmission electron microscopy (TEM)

Transmission electron microscopy (TEM) is a very high resolution microscope, having higher resolution than SEM, which depends on electron beam emitted from an electron gun to transmit through an ultra thin sample (with a carbon grip underneath). The electron beam will be diffracted as it passes through the sample so that a diffraction image and crystalline structure image can be formed, which can be detected by a CCD sensor.[66]

Transmission electron microscopy (TEM, JEOL JEM-2010) was used to determine the diffraction pattern, sample geometry, crystalline structure and the elements of the nanowires. The diffraction patterns of the nanowires were taken by selected area electron diffraction (SAED) method so as to obtain the diffraction pattern of a particular nanowire. Hence, the planar separation and the lattice constants of the nanowires could be calculated. The sample geometries were taken with the typical TEM image to study their lengths and diameters whereas the crystalline lattices were taken with the high-resolution TEM (HR-TEM) image to study their growth direction and the crystalline structures. Energy-dispersive X-ray spectroscopy (EDX) was used to determine the elements of a single nanowire. This is an analytical technique used for the elemental analysis or chemical characterization of a sample by analyzing the X-ray emitted from a sample when it is hit with an electron from the electron gun.[67]

3.4.1 Raman spectroscopy

Raman scattering is a convenient and non-destructive characterization technique for chemical bonding identification, structural characterization, stress analysis and vibration mode detection. This technique bases on the inelastic scattering nature of visible, near

ultraviolet and near infrared light. The Raman spectroscopy works when monochromatic light, usually from a visible laser, incidents on a molecule, it will interact with the electron cloud of that molecule and its bonding. The molecule will be excited to a virtual state by the incident photon. For spontaneous Raman effect, the excited molecule will relax to a lower or higher stationary state accompany with the emission of a photon as shown in Fig. 3.6. The shift in energy gives information about the phonon modes in the molecule. Therefore, by calculating the energy of the final state, the shift of energy of the initial state can be obtained. The frequency shift is called Raman shift and can be described by the following equation:

$$|\hbar\omega_l - \hbar\omega_s|$$

Eq (3.4)

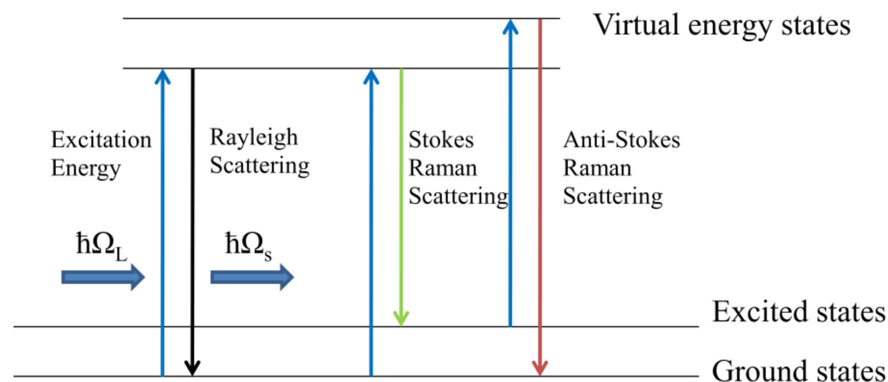

Fig. 3.6 Schematic diagram showing the principle of Raman scattering.

Horiba HR800 Raman spectrometer was used to measure the Raman shift of the nanowires. This spectrometer has a spectral resolution < 0.2 cm^{-1}, which embedded with a 488 nm Ar^+ laser as incident photons for the excitation of specimens. The emitted light

from the sample is collected by a typical microscope via the objective lens from the microscope.

3.5 Optical characterization

3.5.1 Cathodoluminescence (CL)

Cathodoluminescence (CL) is an optical and electrical phenomenon that depends on the emission of a beam of electrons that generated by an electron gun (e.g. cathode ray tube) and then strikes on a luminescent material such as semiconductor or phosphor material. The material is then excited by the electron beams so that the emission of light with corresponding wavelength will be emitted from the material when the excited electrons recombine with certain recombination centers. It is an important technique to study the energy band structures of semiconductors by calculating their band energies from the emission wavelength with the following equations:[68]

$$E = hv$$

(Eq. 3.5)

$$E = h\frac{c}{\lambda}$$

(Eq. 3.6)

CL occurs when there is an impingement of a high energy electron beam onto a semiconductor, which results in the excitation of electrons from the valence band into the conduction band, leaving holes from the valence band. When the electron hole pairs

recombine again, it is possible for photons of the same energy to be emitted. The energy of the photons that emitted, and the probability that a photon can be studied.[69]

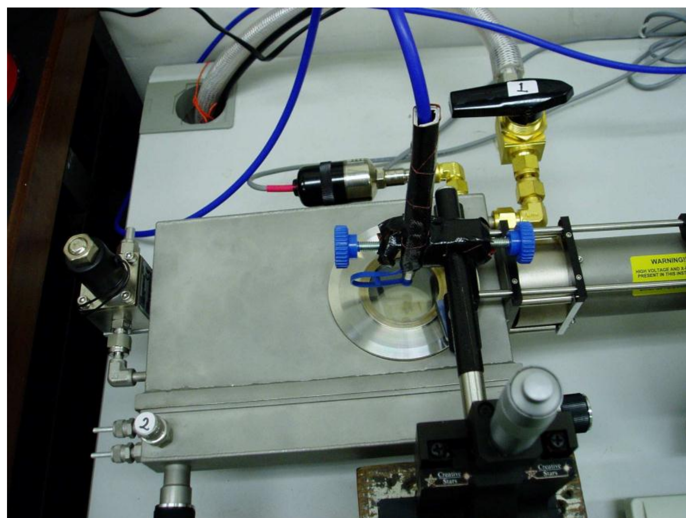

Fig. 3.7 The photo of the CL setup.

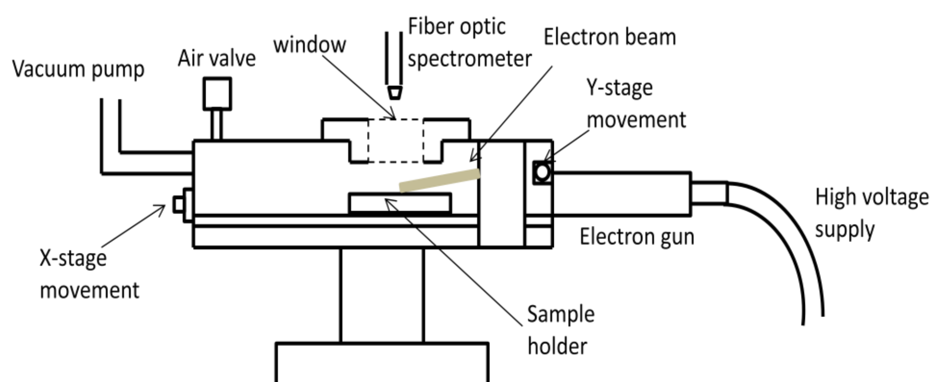

Fig. 3.8 The schematic diagram of the CL setup.

The energy of the electrons that emitted from the electron gun can be adjusted by turning the excitation voltage of the electron gun, which can vary from 1.2 kV to 15 kV. While increasing the voltage, more molecules inside the chamber can be discharged. Hence, the electron gun current will also be increased. During the measurement, the

pressure should be tuned with respect to the change of voltage so that the current can be constant. It is noted that the higher the vacuum, the lower is the current. The vacuum can be tuned by adjusting the air flow into the chamber.

The CL spectra were obtained using a modified Reliotron III CL instrument. The measurement of CL luminescence was divided into two parts. The first part of measurement was carried out using a miniature fiber optic spectrometers (USB 4000, Ocean Optics spectrometer) for the visible light measurement, which couples a 3648-element linear CCD-array detector, a high resolution (0.2 nm) spectrum with range from 350 to 1100 nm. The second part of measurement was carried out using another miniature fiber optic spectrometer (Ocean Optics MayaPro2000 spectrometer) for the deep UV measurement, which couples a back-thinned 2D FFT-CCD detector and a high resolution (~0.035 nm) spectrum with range from 200 to 400 nm.

The CL spectra were taken under the excitation of low-voltage electron beam (4 kV) at the vacuum of 80 mTorr, using an optical fiber to receive the optical signal via a fused silica window on top of the CL chamber as shown in Fig. 3.7. and 3.8. The electron emitted from the electron gun can be focused by two pieces of magnets facing downward on top of the window.

Fig. 3.9 and 3.10 are the detector response curves of the USB 4000 Ocean Optics spectrometer and MayaPro2000 Ocean Optics spectrometer. The USB 4000 spectrometer is most sensitive for detecting wavelength between 500 and 800 nm whereas the MayaPro2000 is able to detect signal between 200 and 400 nm. It is noted that the

detector for the USB 4000 spectrometer is the Toshiba 3648-element TCD1304AP Detector. The resolution of this setup for our measurement is 3 meV per step.

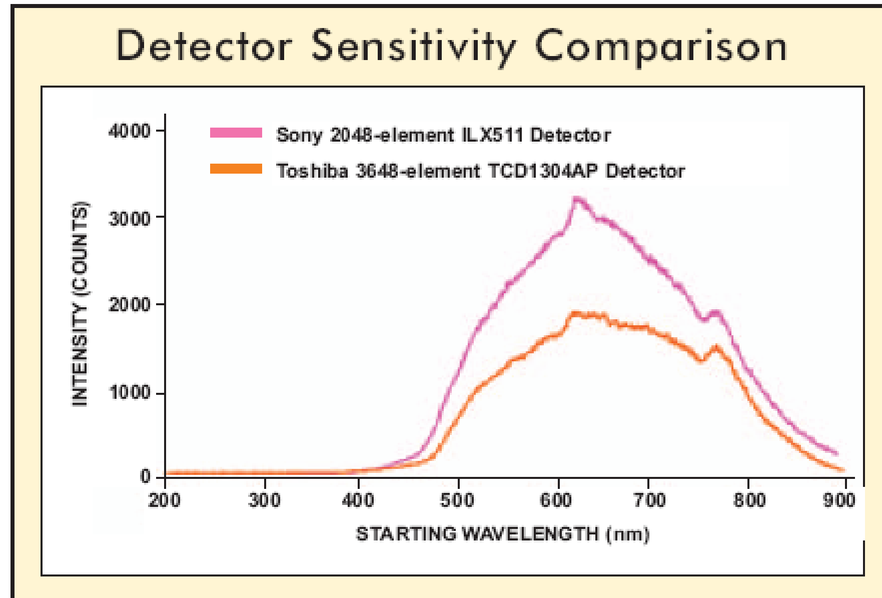

Fig. 3.9 The sensitivity spectrum of the USB 4000 Ocean Optics spectrometer.[70]

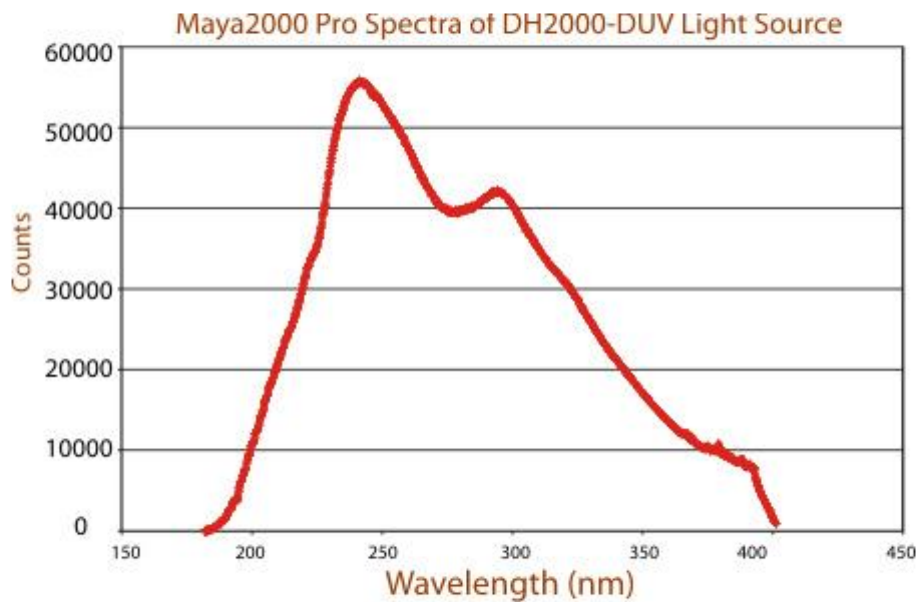

Fig. 3.10 The sensitivity spectrum of the MayaPro2000 Ocean Optics spectrometer.[70]

3.5.2 Photoluminescence (PL)

Photoluminescence (PL) is a process that a semiconducting material absorbs photons generated by either a light source or laser source and then re-radiates photons of the same energy after an electron is excited from valence band to conduction band.[69]

This is one of many forms of luminescences and is distinguished by photoexcitation, which the sample is excited by photon. The period between absorption and emission can be extremely short, for example, in an order of 10 nanoseconds. However, this period can be extended into minutes or hours under special circumstances.[69]

The PL spectra of the nanowires were measured by a femtosecond laser system at Texas Tech University (TTU). Fig. 3.11 shows a complete frequency Quadrupled Ti-sapphire femtosecond laser system. This laser system is specifically designed to generate femtosecond tunable deep UV (195-200 nm) laser light source with 10 mW average power and the signal is collected by a monochromator with gratings operating in the region from 185 - 800 nm, through a PMT, having a resolution larger than 1 nm. This laser system is the world's first DUV ($\lambda > 195$ nm) picosecond time-resolved optical measurement facilities dedicated to III-nitride semiconductor research, and allows users to measure optical processes in AlN up to its band to band emission. The resolution of this setup for our measurement is 6 meV per step.

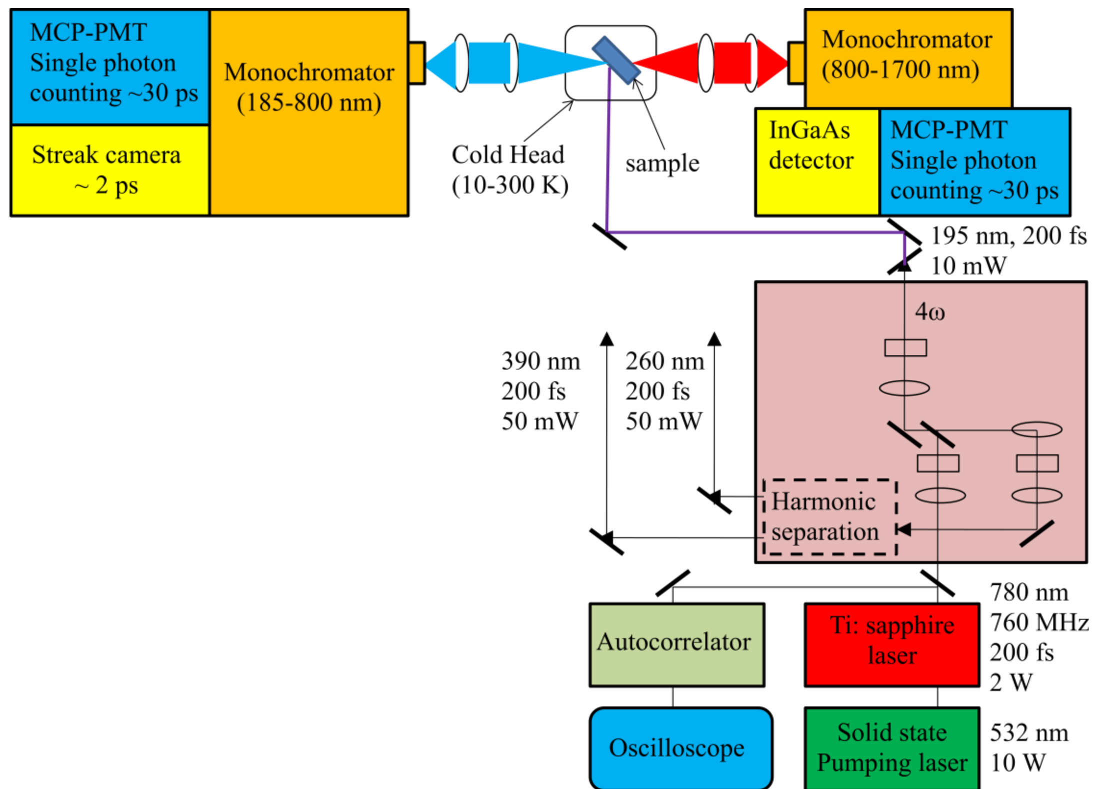

Fig. 3.11 Schematic diagram showing the PL system at TTU.

3.6 Magnetic characterization

3.6.1 Vibrating sample magnetometer (VSM)

Vibrating sample magnetometer (VSM) is an instrument that measures magnetic properties of a sample. When a sample is placed inside a uniform magnetic field, created between the poles of an electromagnet, a dipole moment will be induced. If the sample vibrates with sinusoidal motion, a sinusoidal electrical signal can be induced and detected by a suitable placed pair of pick-up coils. The signal will have the same frequency of vibration as the sample's vibration. Its amplitude will also be proportional to the magnetic moment, amplitude, and relative position with respect to the pair of pick-up coils. The representative schematic diagram of the VSM setup is shown in Fig.

3.12. A Lakeshore 7047 VSM, with sensitivity down to the range of μemu was used for measuring the magnetic properties of the nanowires at room temperature.

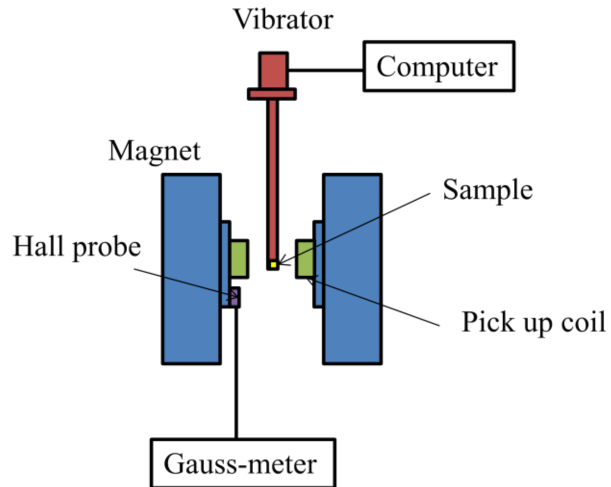

Fig. 3.12 Schematic diagram showing the setup of VSM

Chapter 4 Structural and magnetic properties

4.1 Introduction

AlNNWs and zigzag AlNNWs have been synthesized by the chemical vapor deposition (CVD) method. It is a chemical process that initiates by the chemical reaction of the component chemicals, which are transported to the vicinity of the substrate via the vapor phase. The condensed liquid droplets on the hot substrate are then acting as seeds for the nucleation and growth of single-crystalline nanorods and then nanowires, which differentiate by their aspect ratio.

In this growth process, $MgCl_2$ was acted as catalyst that can initiate the transformation of the reactants into chemical vapors as no nanowires were obtained without the use of $MgCl_2$. The reactant powders were physically mixed together for the generation of vapor species required for the growth of nanowires. AlNNWs were grown on sapphire substrate and alumina tube at the growth temperature of 1450 ^{o}C. Although the source material $MgCl_2$ was used, no Mg dopants were detected in the nanowires. It is noted that the structural properties of the nanowires grown on sapphire and alumina tube were similar. When the growth temperature was set at 1350 °C, AlN nanowires with zigzag morphology was favored, which suggested that Mg dopant could favor the growth of zigzag morphology. About 5 at.% of Mg dopants were detected from the zigzag nanowires by EDX.

No nanowires can be obtained below the temperature 1350 ^{o}C as the temperature is not high enough to vaporize the AlN powder.

4.2 Effect of growth temperature

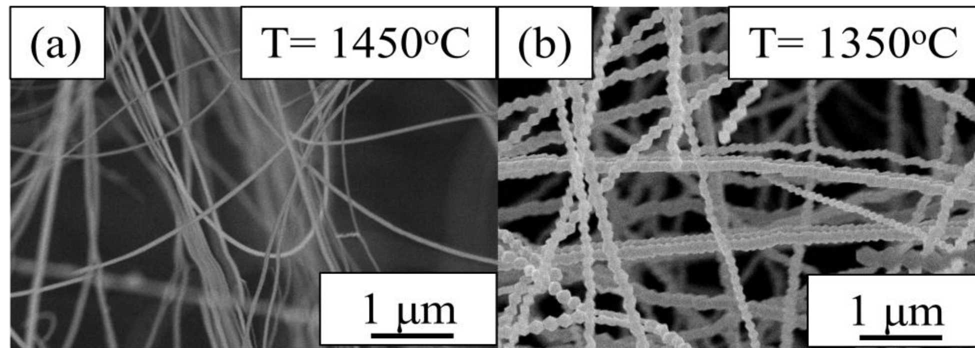

Fig. 4.1 (a) SEM images of the nanowires prepared at 1450 ℃ and (b) zigzag nanowires prepared at 1350 ℃.

Fig 4.1 (a) and (b) show the SEM images of the nanowires and zigzag nanowires grown on sapphire substrates at 1450 and 1350 ℃ respectively. It is found that the growth temperature is crucial to the morphology of the nanowires. When the growth temperature was increased to 1450 ^{o}C, the formation of nanowires was favoured and could be collected from the alumina tube and sapphire substrate provided that the alumina tube was eroded with NaOH. In contrast, the zigzag nanowires were grown on the sapphire substrate when the growth temperature was decreased to 1350 ^{o}C.

4.3 AlNNWs

4.3.1 Effect of growth time

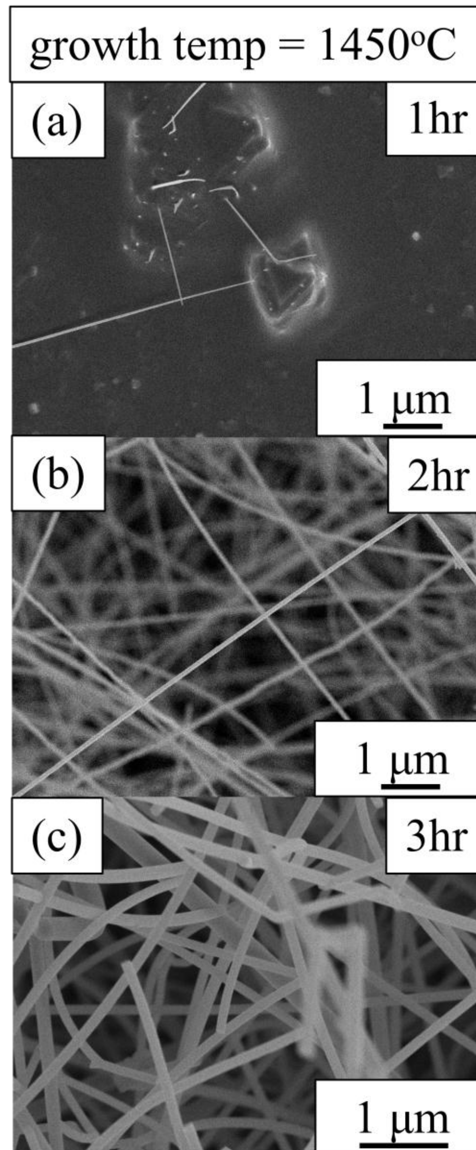

Fig. 4.2 (a) SEM images of the nanowires grown on sapphire substrates at 1450 °C with growth time of 1 hr, (b) 2 hr and (c) 3 hr.

Apart from the growth temperature, the growth time is also an important parameter for the growth of nanowires. It is found that the yield of nanowires increased as the growth time. As shown in Fig. 4.2 (a), only small amounts of nanowires were formed on the sapphire

substrate when the growth time was 1 hr. When the growth time was increased to 2 hr, more nanowires were formed on the sapphire substrate.

4.3.2 Structural properties

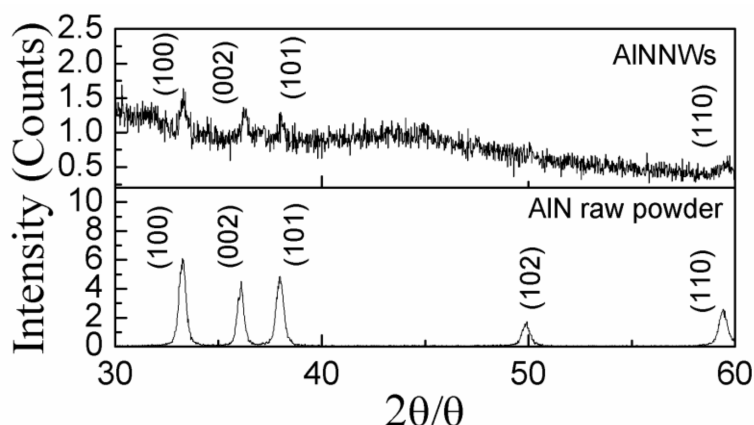

Fig. 4.3 Comparison of the XRD patterns between nanowires and AlN raw powder.

Nanowires were deposited on the inner surface of an alumina tube and a sapphire substrate. It is noted that no nanowires were obtained if no $MgCl_2$ was used.[71] Representative XRD pattern of the nanowires is shown in Fig. 4.3. Several diffraction peaks were observed, which corresponds to the wurtzite h-AlN structure. The broad background was contributed by the carbon tape, which was used to stick the nanowires on the XRD holder. AlN characteristic peaks of (100), (002), (101) and (110) planes can be observed from the XRD pattern. These peaks matched well with the diffraction pattern of the raw AlN powder as shown in Fig. 4.4, which suggests that the nanowires are the direct sublimation product of the raw AlN powder. Moreover, the XRD pattern fitted well with the wurtzite h-AlN structure.[58]

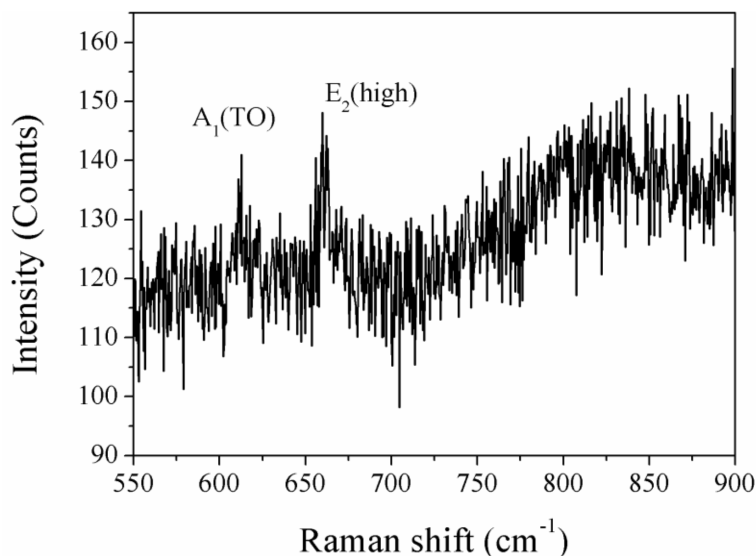

Fig. 4.4 Raman spectrum of the nanowires.

Fig. 4.4 shows the Raman spectrum of the nanowires grown on sapphire substrate. Two characteristic peaks are observed at around 612 and 656 cm^{-1}, which are assigned to the lattice vibration modes A_1 [transverse optical (TO)] and E_2 (high) respectively. The E_2 (high) mode is usually being used to analyze the stress state in the sample due to its high sensitivity to stress. Since the nanowires were free to growth on the substrate, the peak positions of A_1 (TO) and E_2 (high) should fit well with the stress-free bulk AlN crystal.[60]

Moreover, impurities or defects in semiconductors are found to affect the Raman linewidth. Therefore, the contribution of the impurity has broadened the linewidth of the A_1 (TO) and E_2 (high) modes. The weak intensity of the Raman peak indicates the poor crystallinity of AlN. This can be explained by the insufficiency of N ions during the reaction, which can produce a lot of nitrogen vacancies and the N sites eventually being occupied by oxygen. The evidences of oxidation will be shown in the EDX result below.

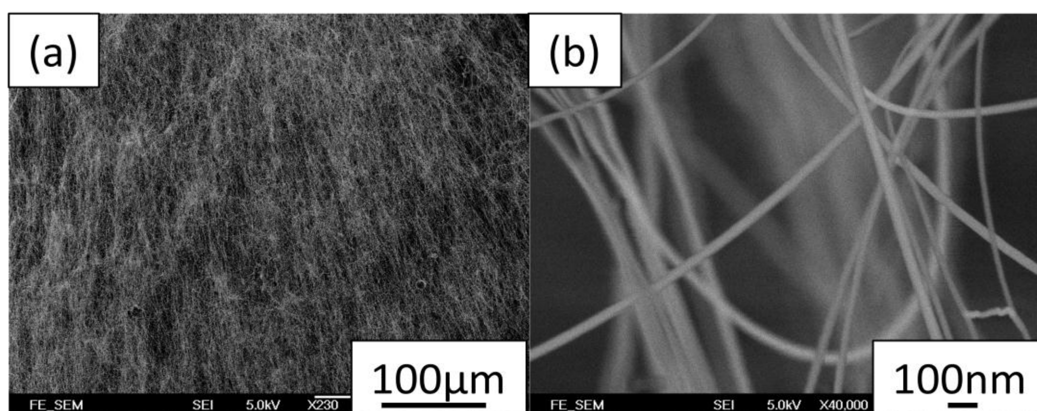

Fig. 4.5 (a) Low and (b) high magnification SEM images of the nanowires.

The SEM images of the nanowires are shown in Fig. 4.5. The nanowires have similar length and diameter, which are grown homogenously on the substrate. The diameters and lengths of the nanowires are ranging from 20-50 nm and 10-50 μm respectively, which have relatively larger aspect ratio when compared with AlNNWs grown from other techniques. Since the nanowires were grown randomly on the substrate, they were grown under a strain-free environment. As a result, the nanowires are dislocation-free and the existence of lattice distortions should be attributed to impurity or dopants.[72]

Fig 4.6 (a) shows the TEM images of the AlNNWs. It reveals a single nanowire with a high aspect ratio of ~100. Fig 4.6 (b) shows a HR-TEM image of one of the nanowires. The nanowire has a single crystalline wurtzite h-AlN structure with *d*-spacing of 2.73 Å ($d_{(100)}$) and 5.00 Å ($d_{(001)}$) between the neighboring lattice planes. This result corresponds well with the XRD pattern obtained above and further confirms the structure of the nanowires. Fig 4.6 (c) shows the selected area electron diffraction (SAED) pattern of the corresponding nanowire. As calculated from the SAED pattern, the lattice constants of the single nanowire are $a = 3.15$ Å and $c = 5.00$ Å with the growth direction along the

[100] direction. These lattice constants are found to be larger than the typical AlN lattice constants (c = 4.98 Å and a = 3.13 Å),[40] which suggests that the nanowires are contaminated with oxygen as no Mg-related peaks can be found from the EDX pattern but an oxygen peak is observed as shown in Fig. 4.6 (d). The small peak cannot be identified as the intensity is too weak to determine its corresponding element. Moreover, the nanowires are obviously Al rich as the Al peak is much stronger than the N peak.

The growth direction of the AlN nanowires is rare when compared with the literatures. Typically AlNNWs grows along the hexagonal *c*-axis as the bonding force is the strongest among all the other directions inside the AlN lattice.[40,58] In our case, the nanowires were grown along the hexagonal *a*-axis, which is the [100] direction. Since no Mg can be observed from the EDX pattern as shown in Fig. 4.6 (d), the lattice distortion of the nanowires should be attributed to the contamination of oxygen but not the doping of Mg. Because of the presence of oxygen, it is possible that the polar surface and the surface diffusion mobility are affected and hence the growth direction along *a*-axis is favored. Jie et al. have confirmed that the growth direction along [100] direction is possible when significantly lower N content is supplied into the system since the surface diffusion mobility on different crystal facets are different for various Al/N ratios and surface polarity.[73]

Indeed, the oxygen contamination is expected as the growth was not performed under high vacuum. Although $MgCl_2$ powder was mixed with the AlN powders, Mg was not detected from the EDX spectrum. As a result, $MgCl_2$ only acted as catalyst during the reaction.

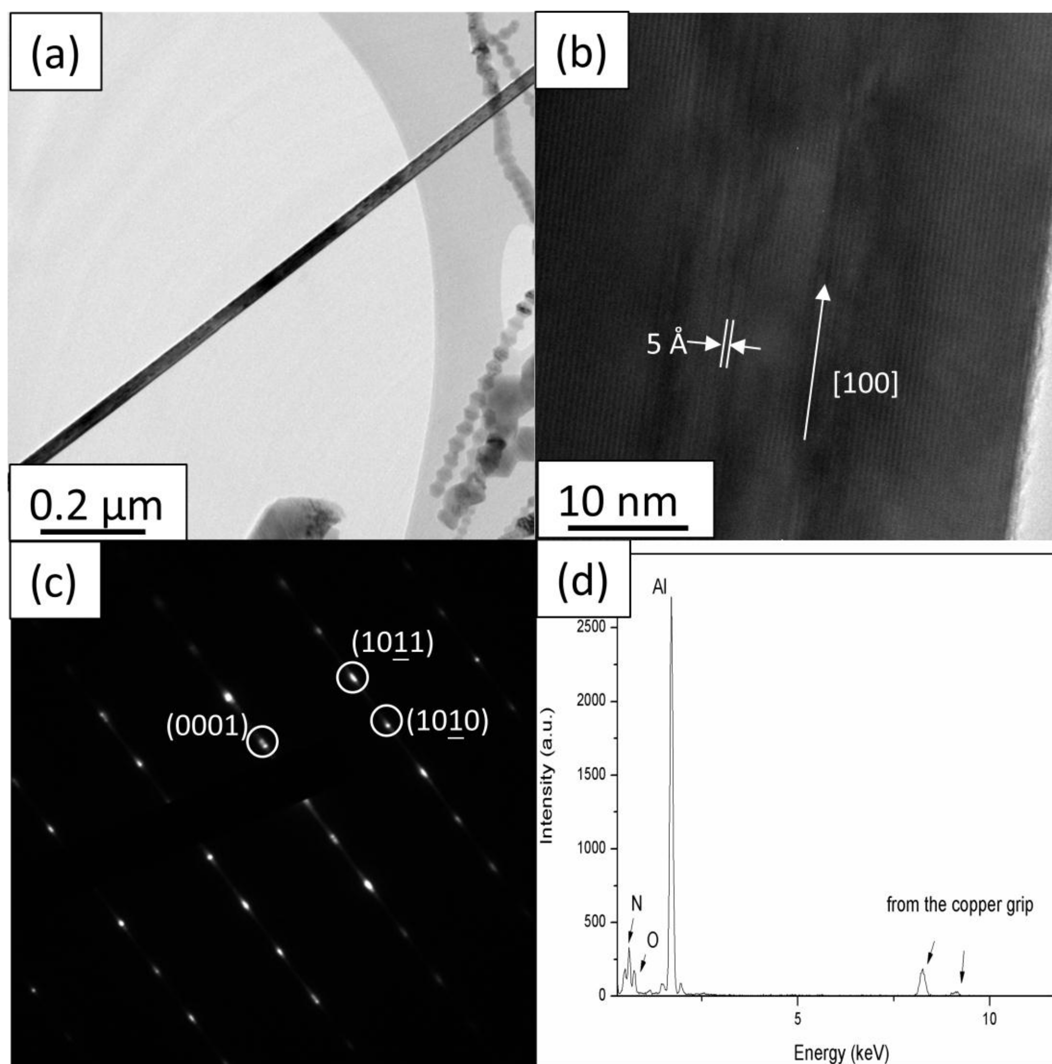

Fig. 4.6 (a) Typical TEM image of a single nanowire. (b) HR-TEM image of the same nanowire showing the crystal lattices. (c) The corresponding SAED pattern. (d) The corresponding EDX pattern obtained by TEM.

4.4 Zigzag AlNNWs

4.4.1 Effect of growth time

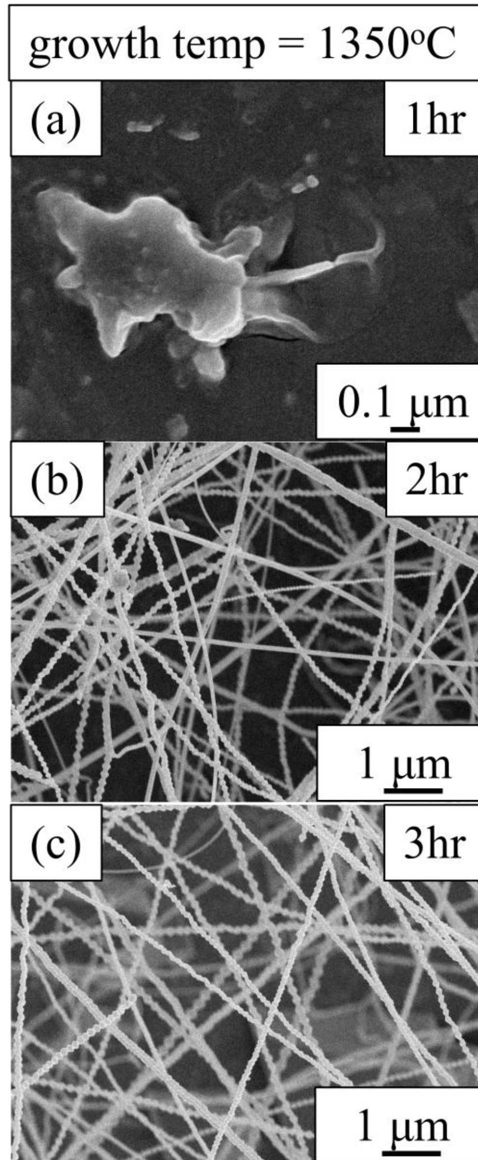

Fig. 4.7 (a) SEM images of the zigzag nanowires grown on sapphire substrates at 1350 °C with growth time of 1 hr, (b) 2 hr and (c) 3 hr.

Similar to the nanowires, the yield of zigzag nanowires also increases with the growth time. As shown in Fig. 4.7, no zigzag nanowires were formed when the growth time was 1 hr. Due to the limited time for the nucleation process, only small amount of AlN

droplets were deposited on the sapphire surface. When the growth time was increased from 1 hr to 2 hr, zigzag nanowires were grown on the sapphire substrate.

4.4.2 Structural properties

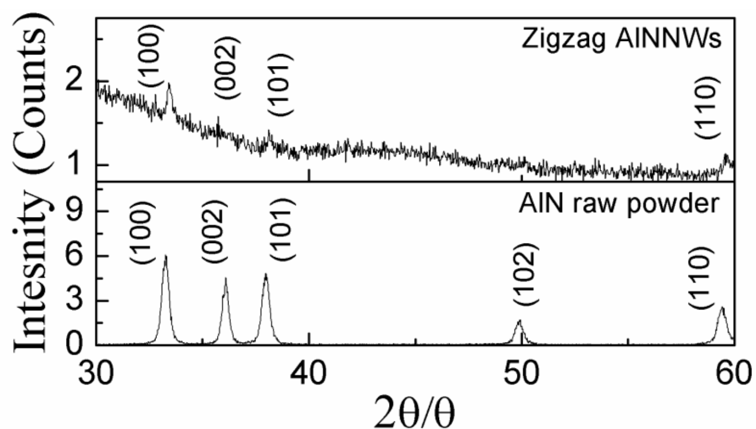

Fig. 4.8 Comparison of the XRD diffraction patterns between zigzag nanowires and AlN raw powder.

Representative XRD pattern of the zigzag nanowires is shown in Fig. 4.8. Diffraction peaks of (100), (002), (101) and (110) planes are observed, which corresponds to the wurtzite h-AlN structure. These peaks fitted well with the diffraction pattern of the raw AlN powder as shown in Fig. 4.8, which suggests that the nanowires are the direct sublimation product of the raw AlN powder.

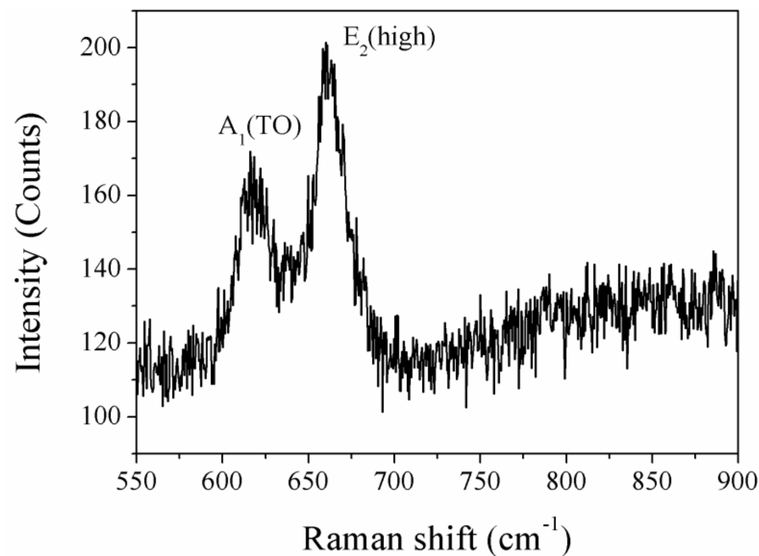

Fig. 4.9 Raman spectrum of the zigzag nanowires.

Fig. 4.9 shows the Raman spectrum of the zigzag nanowires grown on sapphire substrate. Two characteristic peaks are observed at around 616 and 660 cm^{-1}, which are assigned to the lattice vibration modes A_1 (TO) and E_2 (high) respectively. It is noted that the slight shift of these two modes to higher wavenumber can be attributed to the disorder of the crystals due to the incorporation of Mg. The Raman shift indicates the presence of internal stress and the line broadening of the E_2 (high) and A_1 (TO) mode indicates the existence of the defects. In this case, it is due to the presence of Mg and oxygen as the both Mg and O are observed from the EDX pattern below. The shift of the Raman spectrum indicates that the AlN lattices are under an internal stress, which should be attributed to the Mg dopants as the size of Mg atom is larger than that of Al. This result corresponds well with the calculated lattice constants of the zigzag nanowires, which are bigger than the undoped AlNNWs and further proves the existence of Mg dopants inside the AlN lattices.[21]

Typical SEM images of the zigzag nanowires collected from the sapphire substrate are shown in Fig. 4.10 (a) and (b). They reveal randomly aligned zigzag nanowires with high density and high aspect ratio. It is noted that no zigzag nanowires can be obtained from the alumina tube.

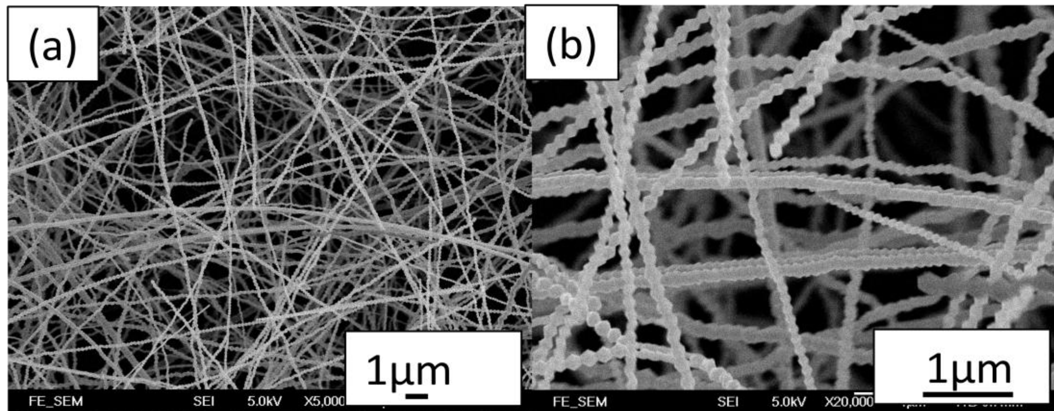

Fig. 4.10 (a) Low and (b) high magnification SEM images of the zigzag nanowires grown on sapphire substrate.

Fig. 4.11 (a) reveals a TEM image of a single zigzag nanowire. Two diameters are defined for the zigzag nanowire. The first diameter (diameter 1) can be defined as the distance between the $(\underline{11}1)$ and $(2\underline{1}3)$ planes. Similarly, the second diameter (diameter 2) can be defined as the distance between the (101) and $(2\underline{13})$ planes as shown in Fig. 4.12 (a). The diameter 1 is estimated to be ~100 nm and the diameter 2 is estimated to be ~80 nm. The length and diameter of the zigzag nanowires are ranging from 10 to 50 μm and 50 to 100 nm respectively. Fig 4.11 (b) shows the HR-TEM image of the corresponding zigzag nanowire. It shows the zigzag nanowire with *d*-spacing of 5.01 Å ($d_{(001)}$) and 2.74 Å ($d_{(100)}$) between the neighboring lattice planes. From the SAED pattern as shown in Fig. 4.11 (c), the calculated lattice constants are c = 5.01 Å and a = 3.16 Å and the growth direction is along [001] direction, which is the hexagonal c-axis.[74] The lattice *d*-spacing

is 5.01 Å between two fringes, which is slightly larger than the lattice constants (*c* = ~4.96 Å, *a* = ~3.12 Å) of the nanowires that synthesized by the other groups.[40] Since both Mg and O peaks are detected from the EDX in Fig. 4.11 (d), it is possible that both of the Mg and O are presented in the AlN lattices and contributed to the lattice distortion because the atomic size of Mg (1.5 Å) is larger than that of Al (1.25 Å).[75] The Mg content in this sample is found to be ~5 at.% as determined by the EDX.

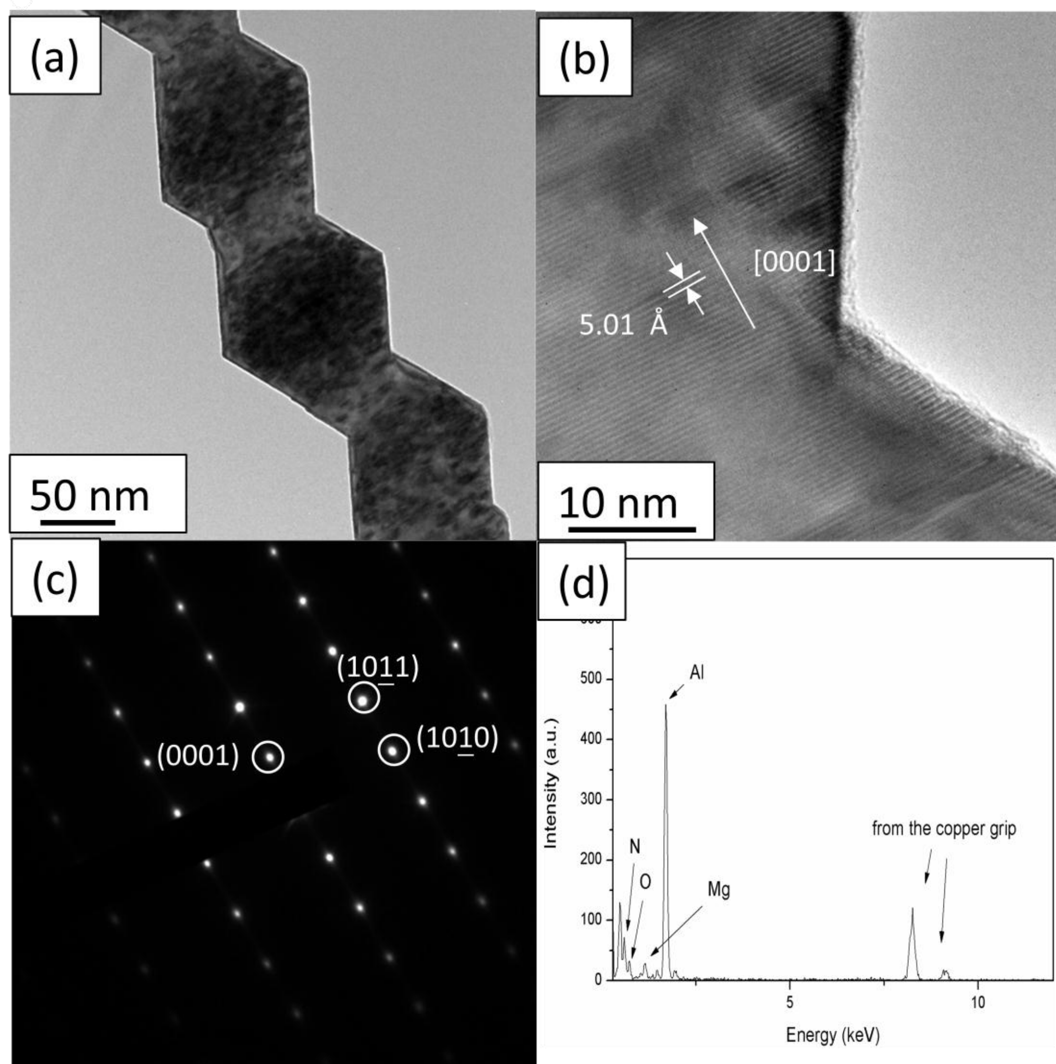

Fig. 4.11 (a) Typical TEM image of a single zigzag nanowires. (b) HR-TEM image of the same zigzag nanowire showing the crystal lattices. (c) The corresponding SAED pattern. (d) The corresponding EDX pattern.

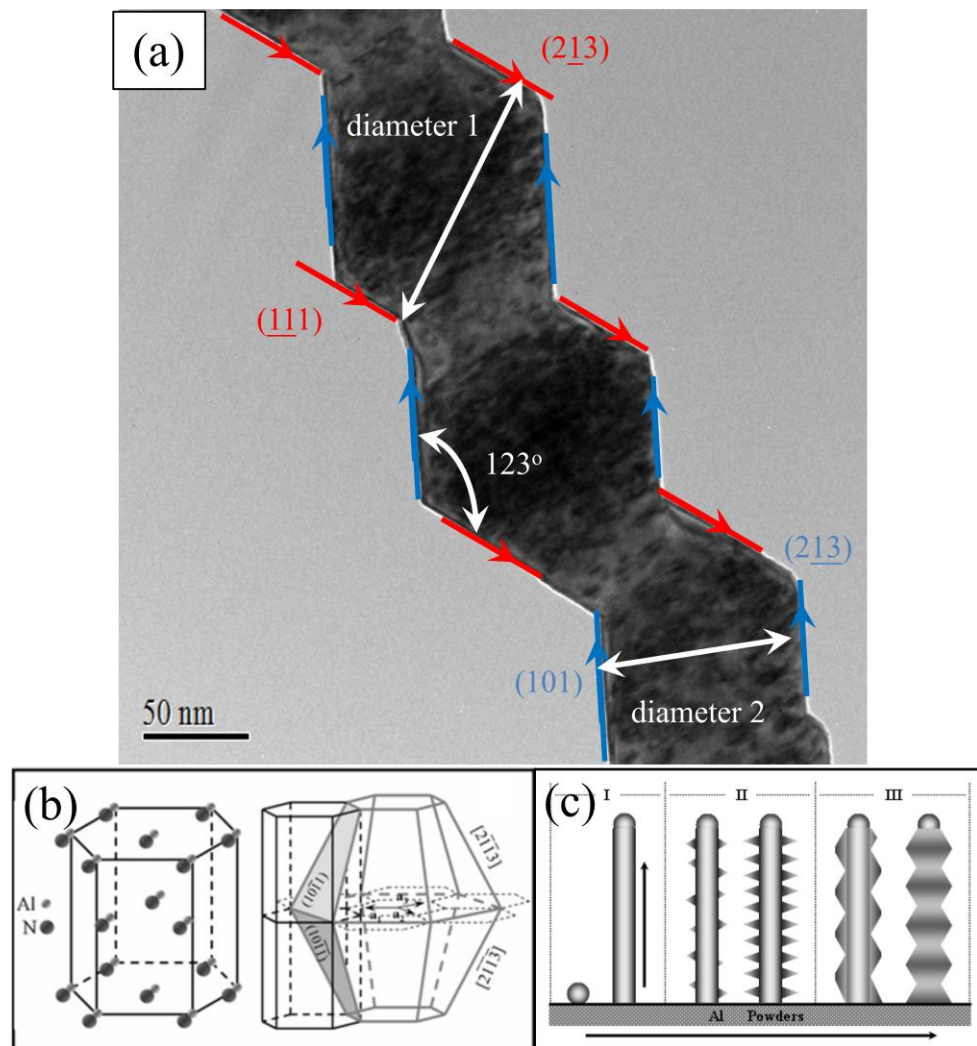

Fig. 4.12 (a) Typical TEM image of a single zigzag nanowires showing the relationship between the turning angles and the surfaces. (b) A structural model of wurtzite h-AlN and the corresponding crystal planes. (c) Schematic diagram showing the growth process of zigzag nanowires.[76]

Fig. 4.12 (b) and (c) illustrate the formation of the zigzag nanowires. Four possible planes can be contributed to the formation of zigzag morphology, which are (101), $(\underline{11}1)$, $(2\underline{13})$ and $(2\underline{1}3)$ planes. It is found that the (101) plane is always parallel to the $(2\underline{13})$ plane as shown by the blue arrows in Fig. 4.11 (b). Similar phenomenon can be observed from the $(\underline{11}1)$ and $(2\underline{1}3)$ planes. Therefore, different zigzag morphology can be established by varying the lengths of these planes. Moreover, the inner angles between two

corresponding edges of the zigzag nanowires are measured to be ranging from 123° to 126° from the HR-TEM iamge. Similar angles can also be calculated using the lattice constants obtained above.

AlNNWs with zigzag morphology has been demonstrated by Wang et al.[82] The suggested growth mechanism of the zigzag nanowires is shown in Fig. 4.12 (c). The formation of zigzag nanowires was found to be related to the growth time. When the growth time was increased from 1 hr to 3 hr, the surface morpologeis of the nanowires were tranformed from nanowires to zigzag nanowires. They suggested that only doped nanowires were able to transform to zigzag nanowires under longer growth time. In our case, similar phenomenon was obsereved as no Mg dopants were observed from the nanowires and Mg dopants were detected from zigzag nanowires only. But the formation of zigzag nanowires was related to growth temperature rather than growth time because the zigzag nanowires were formed at 1350 ^{o}C whrereas the nanowires were formed at 1450 ^{o}C.

On the other hand, extra half planes were introuduced inside the lattices of the zigzag nanowires as shown in Fig. 4.13 (a). The existence of extra half planes can also be proven by the SAED pattern in the inset of Fig. 4.13 (a). There are parellel lines connecting the diffraction spots together. This phenonmenon can be observed when there are stacking faults inside the lattices. Also, it is found that there are variations of the inner angles between two corresponding edges from 123° to 126°. The enlarged image of Fig 4.13 (a) shows one of the extra half planes inside a single zigzag nanowire. It is believed that the Mg dopants introduced some defects and hence intiated the

formation of extra half planes, which ultimately became stacking defects.[77] Fig. 4.13 (b) shows a schematic diagram of how an extra half plane is formed.

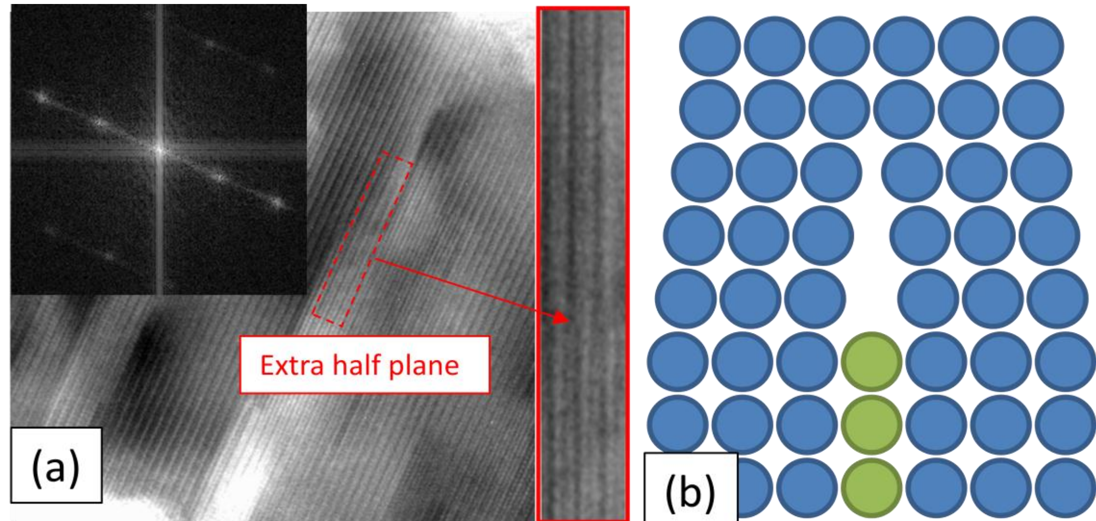

Fig. 4.13 (a) HR-TEM image of a single zigzag nanowire. The inset shows the corresponding electron diffraction pattern. To the right shows the enlarged image of the marked area. (b) Schematic diagram showing the formation of an extra half plane.

4.4.3 Magnetic properties

It is found that no ferromagnetic signal can be detected from the nanowires as no Mg dopants can be observed from those samples in the EDX. However, room temperature ferromagnetism can be observed from the zigzag nanowires, which suggests that Mg can be doped into the AlN lattice and corresponds well with the EDX result. The magnetization versus magnetic field (*M*-*H*) curves of zigzag nanowires with growth time of 2 hr and 3 hr measured at room temperature under applied field parallel (in-plane) and perpendicular (out-plane) to the sample surface are shown in Fig. 4.14.

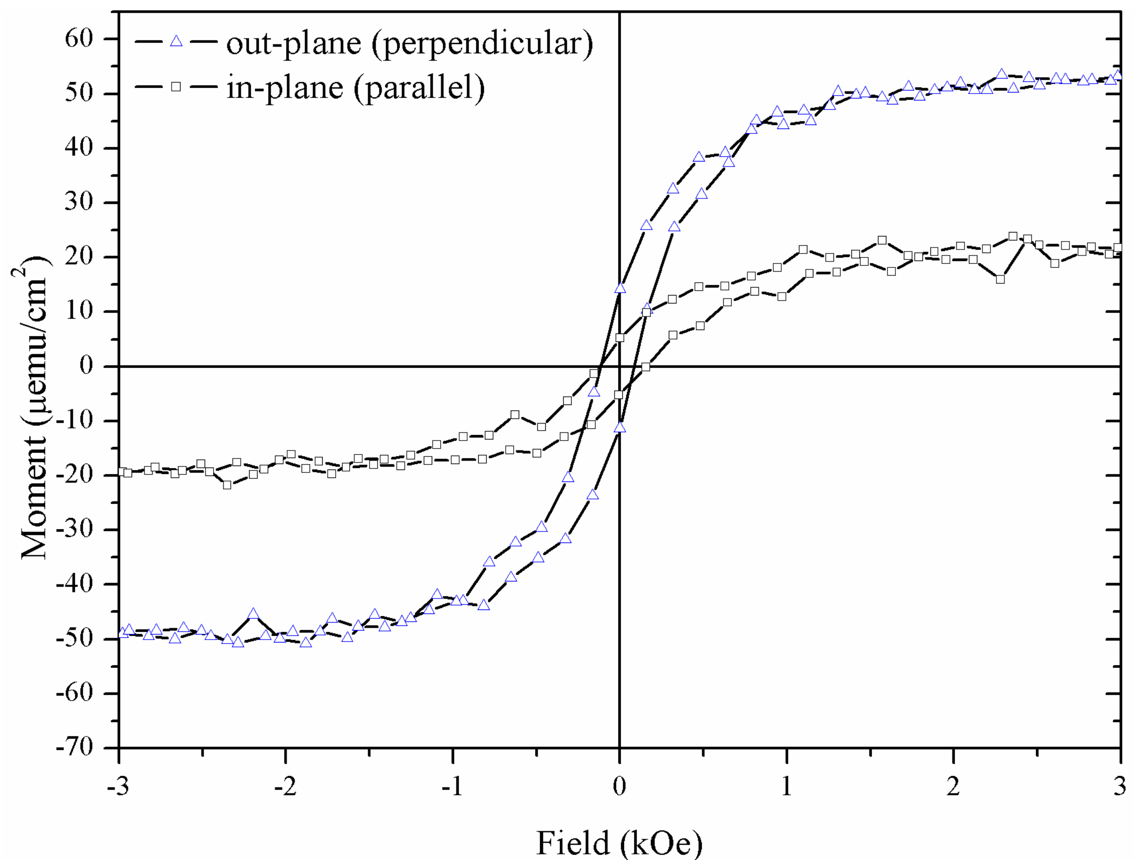

Fig. 4.14 *M-H* loop of the zigzag nanowires grown on sapphire with growth time 2 hr measured at room temperature and applied field parallel and perpendicular to the sample surface.

The spontaneous saturated magnetization and coercivity measured in the *M-H* loop of the zigzag nanowires with samples size of ~40 mm^2 are estimated to be ~50 $\mu emu/cm^2$ and 3 kOe when the field is applied perpendicular to the sample, which is almost 2.5 and 0.2 times larger than the field applied parallel to the sample. The magnetic anisotropy in transition metal (TM) substituted semiconductor is a common characteristic of DMSs. This indicates that a significant fraction of Mg spins are coupled magnetically in AlN. It is noted that both Mg and AlN are intrinsically nonmagnetic. The Mg dopants alone will not contribute to the observed ferromagnetism. As predicted by Wu et al., the room temperature FM in AlN could be obtained if Mg atom

substitute Al site by forming MgN_4 phase. It is calculated by literature that the dipole moment can be induced by the MgN4 phase. This indicates that the zigzag nanowires exhibit intrinsic ferromagnetism.

4.5 Summary

Geometry	Nanowire	Zigzag nanowire
Lattice constant *a* (Å)	3.15	3.16
Lattice constant *c* (Å)	5.0	5.01
Growth direction	*a*-axis of h-AlN	*c*-axis of h-AlN
Growth temperature	1450 ^{o}C	1350 ^{o}C
Vibration modes	612 and 656 cm^{-1}	616 and 660 cm^{-1}
Ferromagnetism	No	Yes

Table. 4.1 Comparison between nanowires and zigzag nanowires.

Table 4.1 has briefly summarized the difference in structural properties between AlNNWs and zigzag AlNNWs. The nanowires and zigzag nanowires have been synthesized by the CVD method. $MgCl_2$ was essential for the growth of nanowires as no nanowires were obtained if no $MgCl_2$ powder was mixed with AlN powder. The zigzag nanowires and nanowires possess similar lattice constants but different growth directions. On the other hand, the growth temperatures of these nanowires were different, see table 4.1.

Nanowires were obtained from inner alumina tube and sapphire substrate at 1450 ^{o}C. The nanowires have lattice constants of *a*=3.15 Å and *c*=5.00 Å with growth direction along the hexagonal *a*-axis [100] direction. No Mg content was detected from the

nanowires. Two vibration modes A_1 (TO) and E_2 (high) located at 612 and 656 cm^{-1} respectively were observed from the Raman spectrum, which fitted well with the stress-free bulk AlN crystal.

Zigzag nanowires were able to grow on sapphire substrate when the growth temperature was set to 1350 ^oC. The zigzag nanowires were doped with Mg as the peak of Mg was detected by EDX. The lattice constants were a = 3.16 Å and c = 5.01 Å with growth direction along the c-axis of wurtzite h-AlN structure. Slight shift of the two vibration modes A_1 (TO) and E_2 (high) to higher wavenumber located at 616 and 660 cm^{-1} respectively were observed from the Raman spectrum, which were attributed by the incorporation of Mg. Also, it is found that the growth time plays an important role in the yield of the nanowires and zigzag nanowires.

Room temperature ferromagnetism was detected from the zigzag nanowires as Mg dopants were observed from the EDX. For this sample with the sample size of ~40 mm^2, the spontaneous saturated magnetization and coercivity were estimated to be ~0.5 $\mu emu/mm^2$ and 3 kOe respectively.

Chapter 5 Optical properties

5.1 Introduction

Owing to the inability of acquiring the near band emission from the undoped AlNNWs, there are different approaches to enhance the optical properties of the AlNNWs. For example, it is believed that the near band emission of AlNNWs can be enhanced by incorporating different dopants into the AlN lattice. Ji et al. demonstrated that the doping of Fe into AlN nanorods can enhance the near band emission of AlN by introducing deep level acceptor states above the valence band of AlN.[21]

The effects of Mg dopants on the optical properties of AlNNWs are studied. The optical properties of AlNNWs and zigzag AlNNWs have been measured by PL and CL. It is found that the nanowires collected from the sapphire substrate and alumina tube possess similar optical properties, which correlated well with the results obtained from previous chapter.

It is found that the oxygen impurities had dominated the PL and CL emissions of the nanowires and zigzag nanowires. Therefore, no near bandedge emissions can be obtained from all the samples. It is noted that the optical properties of the zigzag nanowires were different from that of the nanowires due to the incorporation of Mg dopants. The PL and CL spectra of the zigzag nanowires generally have a redshift as compared with the nanowires. This indicates that the Mg dopant can affect the optical properties of the zigzag AlNNWs.

5.2 AlNNWs

5.2.1 Room temperature PL and CL

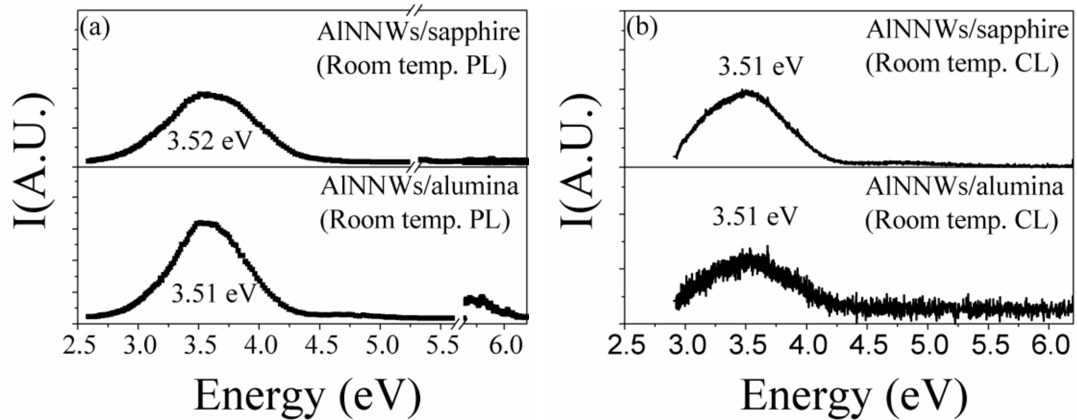

Fig. 5.1 (a) PL spectra and (b) CL spectra of the nanowires grown on sapphire substrate and alumina tube.

As mentioned from previous chapter, upon the synthesis temperature of 1450 ^{o}C, nanowires can be obtained from both alumina tube and sapphire substrate. In order to illustrate the nanowires collected from alumina tube and sapphire substrate possessed similar optical properties, the PL and CL measurement of these samples have been investigated. Fig 5.1 shows the PL and CL spectra of the nanowires deposited on sapphire substrate and alumina tube. A broad PL emission peaks centered at around 3.51 eV can be observed from the nanowires grown on sapphire substrate and alumina tube. Furthermore, both of them possess similar CL emission peaks centered at around 3.51 eV, which corresponds well with the PL emission peaks. This indicates that the nanowires collected from the sapphire substrate and alumina tube possess similar optical properties. The emission peak centered at 3.51 eV is attributed to either oxygen impurity-aluminium vacancy complex (O_N-V_{Al} complex) or oxygen substituting the nitrogen vacancy (O_N), which is related to the creation of defects when oxygen substituted nitrogen in the AlN crystal.[44] It is believed that the concentration of oxygen can vary the position of this peak

from 3.3 to 4.0 eV.[45] In our case, it is more likely that the emission is attributed to the O_N level as the nanowires are Al rich.

The observation of broad spectrum is due to the dominated defect related emissions, which are mostly created by the oxygen, since the solubility of O_2 in AlN lattice can reach several percents and several oxygen-point defect related centers may be formed.[78] Because no active N ions were supplied, large amount of oxygen reacted with the nanowires during the growth. Therefore, when the AlN powder was vaporized, some of the Al ions formed bonding with O ions as the formation energy of Al_2O_3 is lower than AlN.

5.2.2 10 K PL

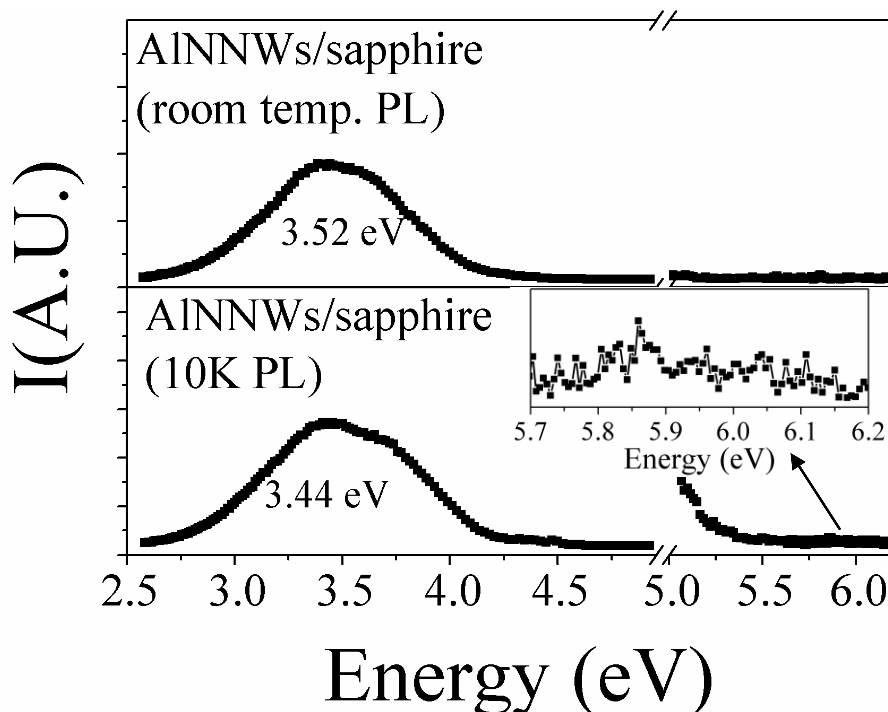

Fig. 5.2 The comparison between the room temperature PL and 10 K PL spectra of the nanowires. The inset shows the magnified image of the 10 K PL spectrum from 5.7 eV to 6.2 eV.

Fig. 5.2 shows the room temperature and 10 K PL spectra of the nanowires. At room temperature, only a broad emission peak centered at 3.52 eV is observed. It is noted that no near bandedge emission can be observed even the spectrum at around 6.0 eV is magnified, which indicates the contamination of oxygen with the AlN lattice can hinder the near bandedge emission. This is due to the oxygen trapped levels created by the oxygen defects. As observed in Fig. 5.2, the defect emission peak is so broad and strong that the trapped level emissions are dominated.

5.2.3 Effect of growth time

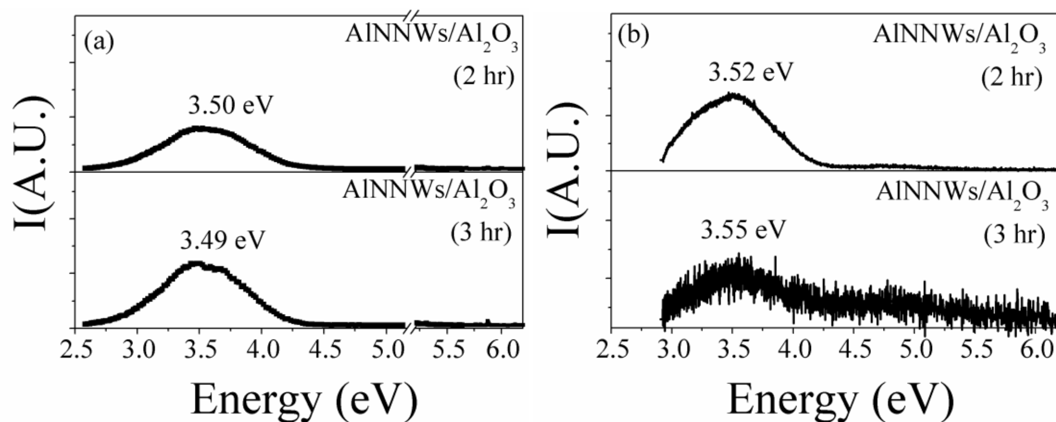

Fig. 5.3 (a) Room temperature PL and (b) CL spectra of the nanowires with growth time of 2 hr and 3 hr.

Fig. 5.3 (a) and (b) illustrate the effect of growth time on the optical properties of the nanowires. As mentioned from previous chapter, only a few nanowires can be grown on the sapphire substrate when the growth time is 1 hr. Therefore, the optical properties of that sample are not studied in this chapter.

It is found that the peak centered at ~3.50 eV from the room temperature PL and CL spectra do not shift as the growth time is increased from 2 hr to 3 hr, which suggests that

the optical properties of the oxygen contaminated nanowires do not change for different growth times. This result correlates well with SEM images obtained from previous chapter as the surface morphology of the nanowires were not changed when the growth time was increased from 2 hr to 3 hr. Since the surface morphology of the nanowires with growth time of 2 hr and 3 hr are similar, the optical properties of these two samples should be similar as well.

5.2.4 Effect of NH_3 annealing

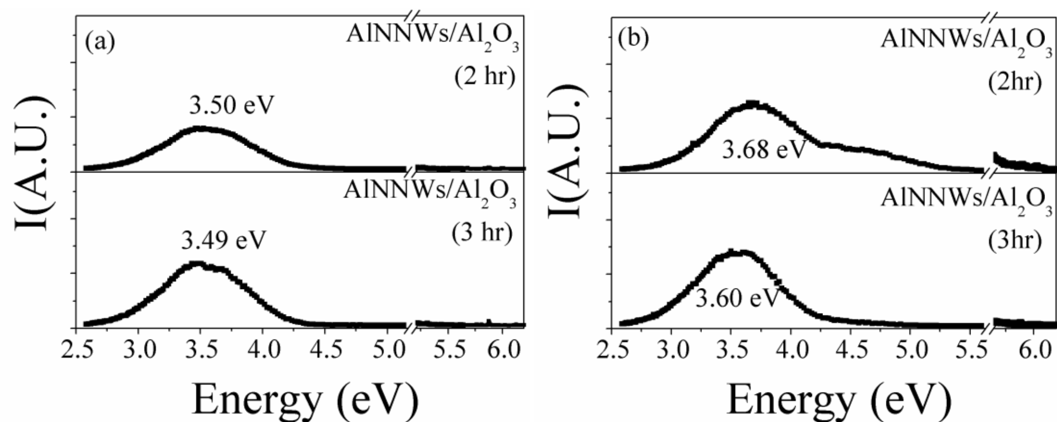

Fig. 5.4 (a) PL spectra of the nanowires synthesized at 1450 ^{o}C with growth time of 2 hr and 3 hr. (b) PL spectra of the corresponding nanowires annealed at 900 ^{o}C under the flow of ammonia (NH_3) gas for 2 hr.

It is reported that upon annealing of AlNNWs with ammonia gas (NH_3), the defect emission peaks of the nanowires can be suppressed by removing the nitrogen vacancies (V_N) inside the AlN lattices. They suggested that the V_N can be suppressed by annealing the nanowires at 875 ^{o}C for 2 hr.[56] Therefore, by similar approach the nanowires were annealed in a tube furnace with NH_3 gas at 900 ^{o}C for 2 hr. It is found that the defect emission peaks of the nanowires did not change after the annealing process. The inability to suppress the emission peaks can be explained by the contamination of

oxygen of the nanowires. Since the samples were synthesized in low vacuum condition and high temperature, oxygen could easily incorporate into the V_N sites inside the AlN lattices. The oxygen can replace the V_N easily as the formation energy of Al-O is lower than that of Al-N so that there are no effects on the annealing of the nanowires.[58]

5.3 Zigzag AlNNWs

5.3.1 Room temperature PL and CL

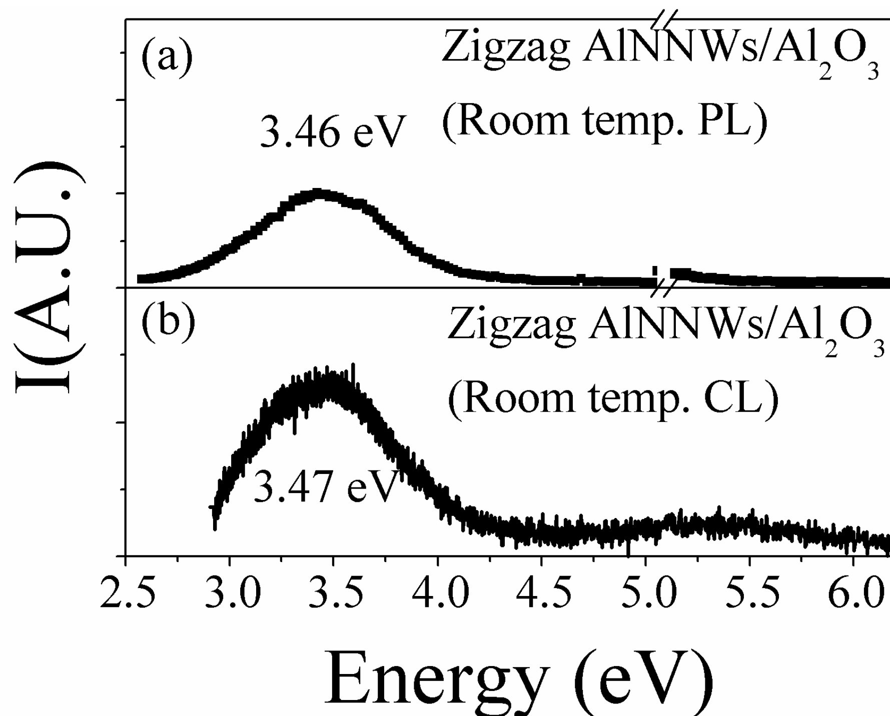

Fig. 5.5 (a) The PL and (b) CL spectra of the zigzag nanowires grown on sapphire substrate.

Fig 5.5 shows the optical properties of the zigzag nanowires grown on sapphire substrate. Similar to the PL result obtained from the nanowires, there are no near band emissions and only a strong and broad defect emission band centered at ~3.46 eV can be detected from the PL spectrum. It is noted that the emission peak positions of the zigzag nanowires are generally lower than that of the nanowires. There are two possibilities for the shift of

this emission peak position. First, as mentioned above, the emission peak centered at 3.46 eV is attributed to the oxygen impurity substituting nitrogen vacancies, and the concentration of oxygen can change the position of this peak from 3.3 to 4.0 eV.[45] Since the growth temperature for the nanowires and zigzag nanowires are different, the concentration of oxygen in the AlN lattice could be different as well.

Second, as obtained from the EDX result, Mg dopants are detected in the zigzag nanowires. They may act as deep level acceptors to accept the electrons transited from the oxygen trapping levels and serve as recombination sites for the electrons transmitted from the conduction band. Similar result has reported by Jing's group in AlN thin-film system. They measured the deep acceptor level (Mg^o) to be 0.50 eV above the valence band of AlN.[6] In our case, the Mg-doped zigzag nanowires and undoped nanowires have a difference of (3.52 – 3.46 eV = 0.06 eV) 0.06 eV in transition energy only, which is ~10 times smaller than their measured value. The energy difference can be explained by the incorporation of oxygen impurities. Since oxygen impurities are incorporated into the AlN lattice as mentioned in the EDX results, it is possible that the Mg may form complex with O so that the Mg and O are co-doped into the AlN lattice. As a result, the Mg^o acceptor level is shifted. The shift of oxygen defect emission peaks from the Mg-doped samples gives another strong evidence for the successful doping of Mg into the AlN lattice.

Apart from the PL spectrum observed in Fig. 5.5, it is found that only one emission peak can be obtained from the CL spectrum, which is centered at 3.47 eV. The emission peak

centered 3.47 eV obtained from the CL spectrum correlates well with the emission peak centered at 3.50 eV from the PL spectrum.

5.3.2 10 K PL

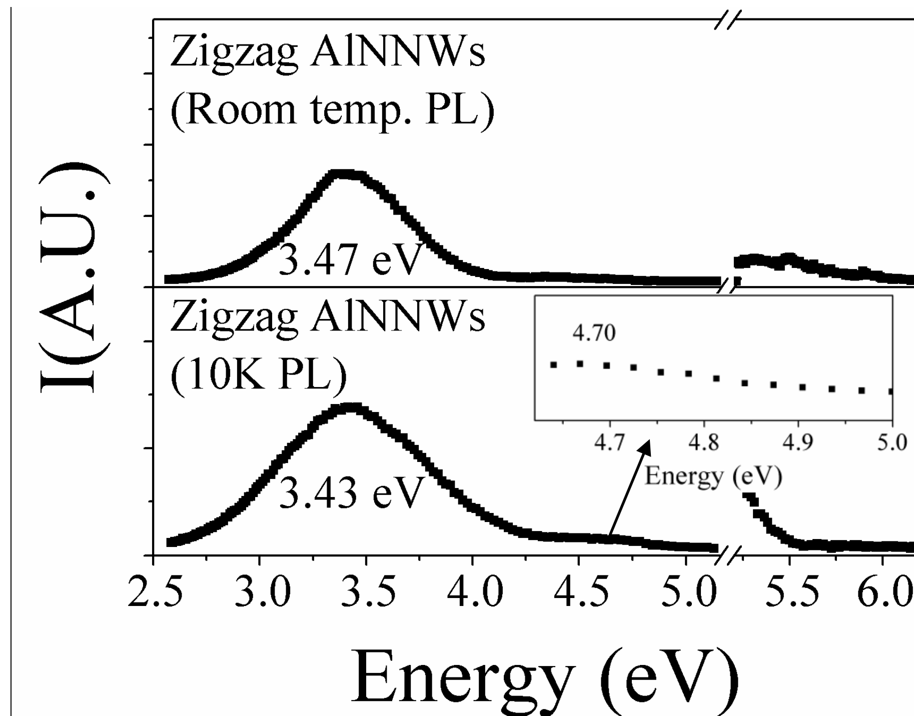

Fig. 5.6 Room temperature PL and 10 K PL spectra of the zigzag nanowires. The inset shows the magnified image of the 10 K PL spectrum from 4.62 eV to 5 eV.

In Fig. 5.6, a possible emission peak centered at 4.7 eV is observed from the PL spectrum measured at 10 K. Since this emission peak is broad and weak, the origin of this peak cannot be explained. However, this emission peak may be attributed to the transmission from the nitrogen vacancies (V_N^{3+}) to the Mg^o. Since the formation energy of nitrogen vacancy with three positive charges (V_N^{3+}) is smaller than that with one positive charge (V_N^{1+}). Thus, the generation of V_N^{3+} is more favourable during the growth of zigzag

nanowires and the V_N^{3+} deep donors can compensate free holes in acceptor-doped materials.[6] However, no near bandedge emission can be observed from this sample even at 10 K as the oxygen related defects are still dominant such that the oxygen acted as electron trapped levels to hinder the direct transmission of electrons from conduction band to Mg^o. Thus, no near bandedge emission can be observed even at low temperature. As a result, a high vacuum ambient for the synthesis of zigzag AlNNWs is desirable.[6] It is noted that the shoulder located at around 5.5 eV in PL measurement could not be identified as it disappears at 10 K PL measurement

5.3.3 Effect of growth time

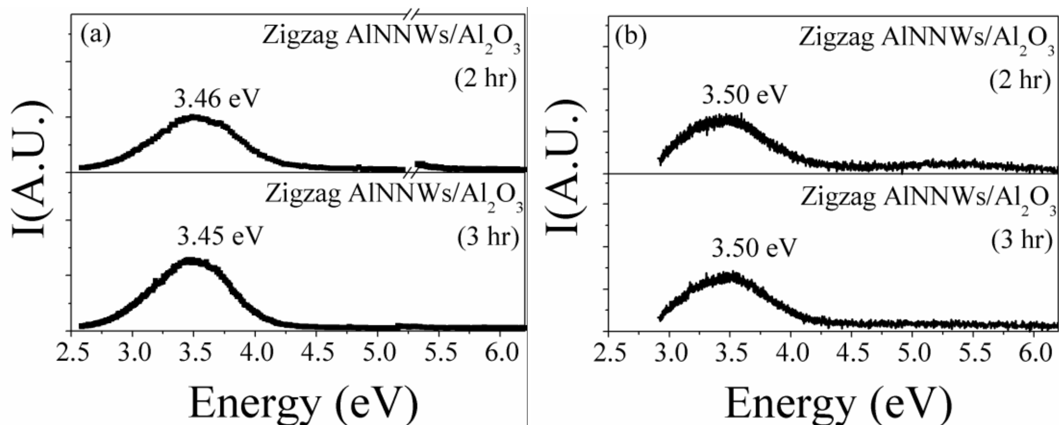

Fig. 5.7 (a) Room temperature PL spectra and (b) CL spectra of the zigzag nanowires synthesized at 1350 °C with growth time of 2 hr and 3 hr.

Fig. 5.7 shows the room temperature PL and CL spectra of the zigzag nanowires. The oxygen related emission peak centered at ~3.46 eV are observed from the samples with growth time of 2 hr and 3 hr. This result correlates well with SEM images as the surface morphology of the zigzag nanowires were changed when the growth time was increased from 2 hr to 3 hr. Since the surface morphology and growth condition of the zigzag

nanowires with growth time 2 hr and 3 hr are similar, the optical properties of these two samples should be similar as well.

5.3.4 Effect of NH_3 annealing

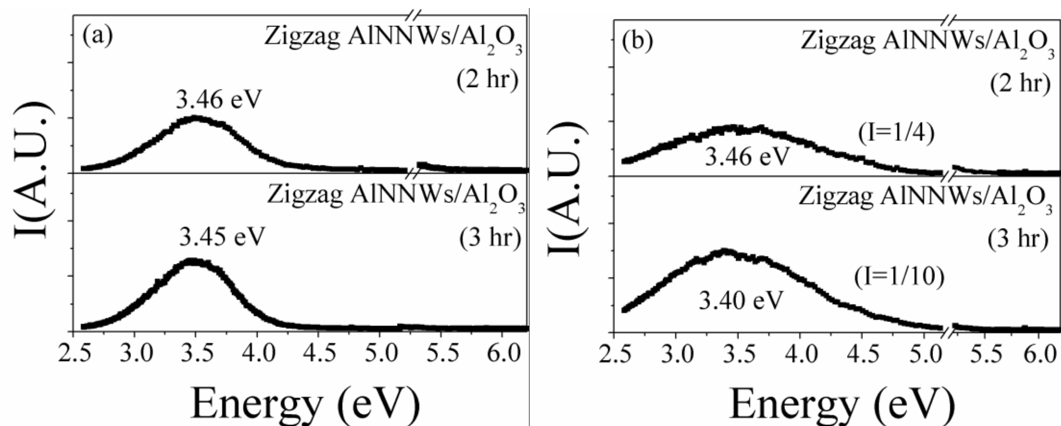

Fig. 5.8 (a) PL spectra of the zigzag nanowires synthesized at 1350 ^{o}C with different growth time of 2 hr and 3 hr. (b) PL spectra of the annealed zigzag nanowires synthesized at 900 ^{o}C under the flow of NH_3 gas for 2 hr.

The zigzag nanowires were annealed in NH_3 gas at 900 ^{o}C for 2 hr and the corresponding PL spectra are shown in Fig. 5.8. It is found that oxygen defect related emission peak can be successfully suppressed after annealing. The intensity of the defect emission peaks can be reduced by 4 to 10 times of the original magnitude and the peak is broadened. Moreover, the position of the defect emission peak has not changed much, which suggests that this emission peak originated by oxygen trapped level defect emissions. Although the defect emission peaks are suppressed, no near band emissions can be obtained, which suggests that the oxygen trapped levels still dominated the transition process.[56]

5.4 Summary

The optical properties of the nanowires and zigzag nanowires were analyzed by PL and CL. For the nanowires, only a broad oxygen defect related emission peak centered at ~3. 50 eV was obtained. The defect was believed to be the O_N level as the nanowires was Al rich but lack of N as no active nitrogen sources were supplied to the growth of nanowires. Moreover, no near band emission was observed from the 10 K PL spectrum.

The zigzag nanowires were found to possess different optical properties as compared to AlNNWs. They were found to have oxygen related defect emission peak centered at ~3.47 eV. Furthermore, a possible emission peak centred at 4.7 eV was observed from the PL spectrum at 10 K. This emission peak was attributed to the transmission from the V_N^{3+} to the Mg^o level, which further demonstrated the successful doping of Mg. Upon the annealing with NH_3 gas at 900 ^oC for 2 hr, the oxygen related defect emission peak position was not changed but the intensity was suppressed a few times of the original value.

The PL and CL spectra of the nanowires were generally located at higher energy level. Therefore, there were small differences between the PL spectra of the nanowires and zigzag nanowires. There were two possible reasons for the difference. First, this small difference could be explained by the Mg dopants inside the zigzag nanowires. Second, since the growth temperature of the nanowires and zigzag nanowires were different, the oxygen concentration could be different.

Chapter 6 Lighting emitting device (LED)

6.1 Introduction

Although the optical properties of the AlNNWs in this project were not as good as expected, a strong UV emission peak can still be obtained from all the samples and it is quite stable. Therefore, an AlNNWs/*p*-SiC heterojunction LED was synthesized using the growth method as mentioned in chapter 4. The only difference in the growth process is that a *p*-doped 4H-silicon carbide (*p*-SiC) substrate (the polished surface faces up) with the size of 0.5 cm by 0.5 cm was placed onto a sapphire substrate so as to protect the *p*-doped surface of the *p*-SiC substrate from any deposition. The growth was maintained at 1450 ^{o}C for 2 hr and a layer of randomly aligned nanowires with a few microns thick was formed on the surface of the *p*-SiC substrate.

Since the growth temperature was 1450 ^{o}C, AlNNWs were grown on the *p*-SiC substrate to form a heterojunction LED. The advantage of using this growth temperature is that this temperature can grow nanowires with higher yield and the nanowires can be collected from all around the inner alumina tube. Therefore, nanowires can be grown easily on the surface of the *p*-SiC substrate.

6.2 Fabrication

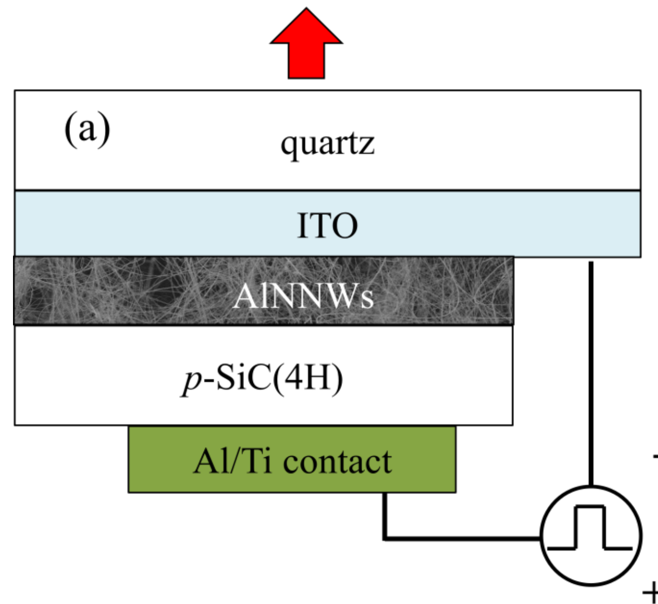

Fig. 6.1 Schematic diagram showing the heterojunction LED.

Fig. 6.1 shows that schematic diagram of the heterojunction LED. The *p*-SiC substrate is chosen as the hole injection layer of the heterojunction because it has high hole concentration (~1×10^{19} cm^{-3}) and carrier mobility (~120 cm^2/Vs) and *p*-SiC substrate does not support radiative recombination at visible regime. The contact of the heterojunction was fabricated by depositing a metal layer of dimension about 2×2 mm^2, which consisted of a layer of ~25 nm thick Al film and a layer of ~150 nm Ti film. They were deposited on the back of the *p*-SiC substrate, by electron-beam sputtering so as to create an Ohmic contact with the *p*-SiC substrate. The sample was then subjected to rapid thermal annealing at 800 ^{o}C in N_2 gas for 5 min in order to obtain a linear current-voltage dependence of the Al/Ti metal contact on the *p*-SiC substrate.[79] After that, a piece of indium tin oxide (ITO) coated quartz substrate was clamped on top of the nanowires in order to cover the nanowires and to avoid direct deposition of ITO onto the nanowires.

This is because the deposition of ITO may penetrate through the gap of the randomly packed nanowires into the *p*-SiC substrate to induce a small shunt resistance to the device. Hence, the ITO film coated onto the quartz substrate was used as the transparent conducting layer of the LED as UV is allowed to pass through ITO and quartz.

6.3 Structural properties

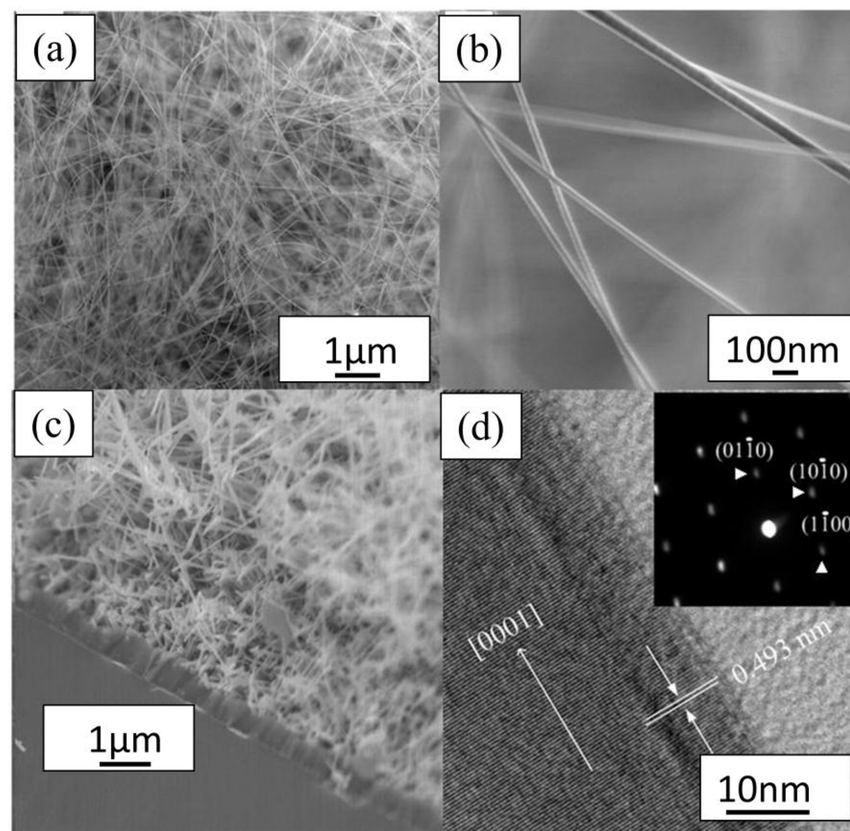

Fig. 6.2 (a) A typical SEM image of the randomly packed nanowires. (b) A magnified SEM image of a single nanowire. (c) Cross-section SEM image of the interface between nanowires and *p*-SiC substrate. (d) HR-TEM image of a single nanowire and the inset shows the corresponding SAED pattern.

Fig. 6.2(a) shows a top view SEM image of the randomly packed nanowires grown on *p*-SiC substrate. The magnified SEM image of a single nanowire is shown in Fig. 6.1(b).

It is observed that the nanowires are grown homogenously on the substrate with very high aspect ratio, having average length of a few microns and diameters of smaller than 100 nm. Due to the high aspect ratio, the nanowires are able to closely packed together to form a thin film like structure on top of the substrate. Fig. 6.1(c) shows the cross-sectional SEM image of the heterojunction. It is noted that the nanowires are randomly grown on the surface of the *p*-SiC substrate with thickness of a few microns. Fig 6.1(d) shows a HR-TEM image of a single nanowire and the inset indicates the corresponding SAED pattern. The crystallinity of the nanowire is good as the surface of the nanowire still shows crystalline structure with smooth surface. It is verified that the nanowire is composed of AlN with wurtzite hexagonal structure. The lattice spacing is 0.493 nm in the growth direction corresponds to the [001] plane of wurtzite h-AlN.[80] It is noted that the growth direction of the nanowires grown on SiC substrate is along the [001] direction, which is different from the [100] direction of the nanowires grown on sapphire.

6.4 Electrical properties

It can be shown in Fig. 6.3(b) that a nearly Ohmic contact is formed on the *p*-SiC substrate and the corresponding resistance is about 2 kΩ. The Ohmic contact of the nanowires can be obtained by depositing a ~200 nm thick ITO layer onto the surface of the randomly packed nanowires via electron-beam sputtering at room temperature. Fig. 6.3 (a) plots the current-voltage (*I*-*V*) curve of the heterojunction. It is observed that the heterojunction has a turn-on voltage of ~8 V, which is close to the bandgap of AlN (~6.0 eV). In order to show that the *I*-*V* behavior is mainly due to the heterojunction, *I*-*V* curves of the two ITO contacts with different separations (d = 200, 500, 800 μm) deposited on

the surface of the randomly packed nanowires are measured. Although the *I-V* characteristic is not perfectly linear, when the absolute voltage below 15 V, the relationship between *I* and *V* is roughly linear as obtained in Fig. 6.3 (b). Moreover, the *I-V* characteristic from Fig. 6.3 (a) is asymmetric, which gives a turn on voltage at about 8 V, and light can be obtained only under the forward bias. Hence, the rectifier behavior below 15 V obtained from Fig. 6.3 (a) is originated in the heterojunction but not the Schottky barrier between the contact electrodes and the nanowires.

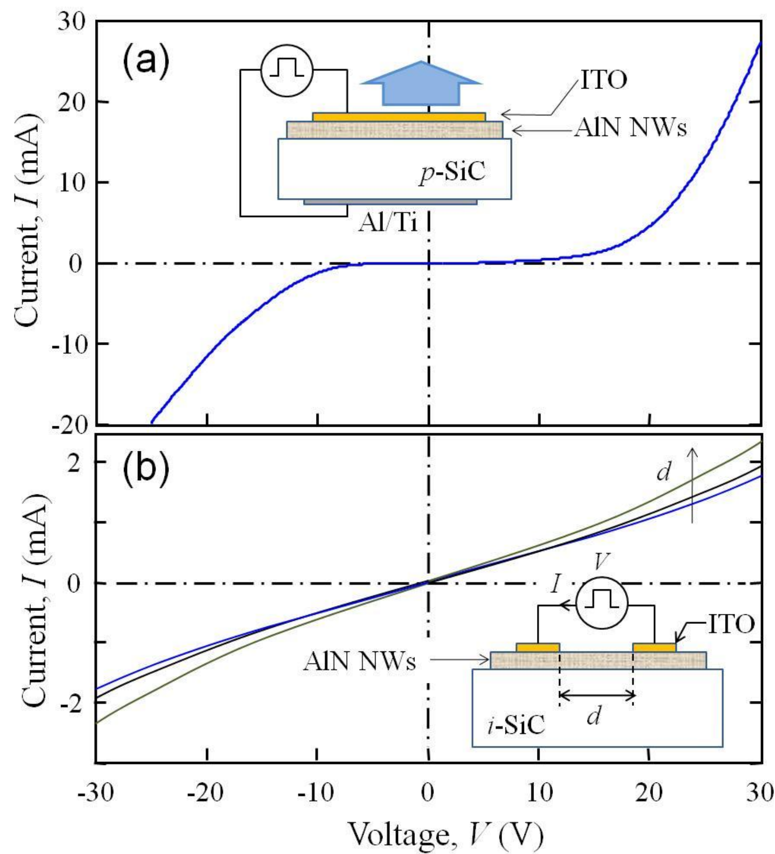

Fig. 6.3 (a) Room-temperature *I-V* characteristics of the heterojunction LED. The inset shows the schematic diagram of the proposed heterojunction LED. (b) Room-temperature *I-V* curves of two ITO contacts deposited on a layer of randomly packed nanowires. The inset shows the corresponding measurement setup.

6.5 Optical properties

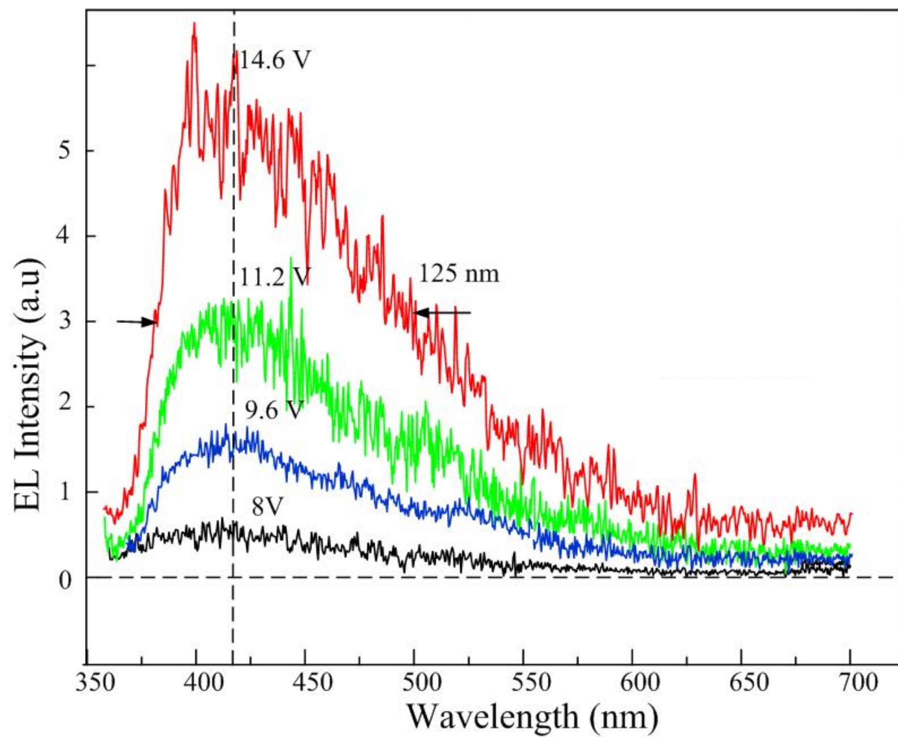

Fig. 6.4 Room-temperature EL spectra of the heterojunction LED under bias voltages of 8 V, 9.6 V, 11.2 V and 14.6 V.

Fig. 6.4 shows the electroluminescence (EL) spectra of the heterojunction LED under forward bias at different voltages, which are 8 V, 9.6 V, 11.2 V and 14.6 V. The spectra were measured by connecting the cathode and anode to a rectangle pulse voltage source, which had a repetition rate and pulse width of 7.5 Hz and 80 ms. The anode was connected to the ITO, whereas the anode was connected to the Al/Ti metal contact of the heterojunction. The emitted light from the sample surface was collected from the surface of the ITO quartz by an objective lens. Full width of half maximum (FWHM) of about 125 nm was calculated when the forward bias was increased up to 14.6 V. No light emissions were observed from the heterojunction LED under reverse bias. This gives a very strong proof on the rectifying properties of the LED. Strong light emission from the

surface of the LED was detected at the region right below the metal contact, due to a higher radiative recombination dominated in the sandwiched region between the contacts when a more intense electric field was applied to the closely packed nanowires. It is shown in Fig. 6.4 that the light emission increases proportionally with the applied voltage and a broad emission peak centered at around 420 nm is observed.

Fig. 6.5 (a) plots the fitting results of the EL spectrum recorded at forward bias (14.6 V) from the heterojunction LED. It is found that the emission spectrum can be fitted by four Gaussian curves with peak wavelength at ~400, ~420, ~468 nm and ~525 nm. Furthermore, the positions of the four peaks were not changed by more than ~4 nm for the variation of bias voltage above the turn-on voltage. Therefore, the nanowires can be considered to have four radiative recombination centers. Fig 6.5(b) plots the photoluminescence (PL) spectrum of the randomly packed nanowires deposited on the *p*-SiC substrate. The emitted light was collected in the direction perpendicular to the surface of the randomly packed nanowires.

A broad emission peak can also be observed from the PL spectrum and the fitting results of the PL spectrum are also shown in Fig. 6.5(b). The emission peak can also be fitted by four Gaussian curves with peak positioned at ~398 nm, ~425 nm, ~470 nm and 525 nm. These values are close to those values observed from the EL spectrum. Since the PL result corresponds well with the EL result and the sum of four Gaussian peaks fitted well with the EL peak as shown in the inset of Fig. 6.5 (a), it has verified that there are four recombination centers, which corresponds to the four emission peaks responsible for the radiative recombination inside the nanowires.

It is noted that the optical properties of the nanowires grown on *p*-SiC is different from that of the nanowires grown on sapphire substrate. For the nanowires grown on *p*-SiC substrate, four Gaussian peaks centered at 398, 425, 470 and 525 nm are obtained from the PL spectrum, whereas only one emission peak centered at 354 nm is obtained from the nanowires grown on sapphire substrate.

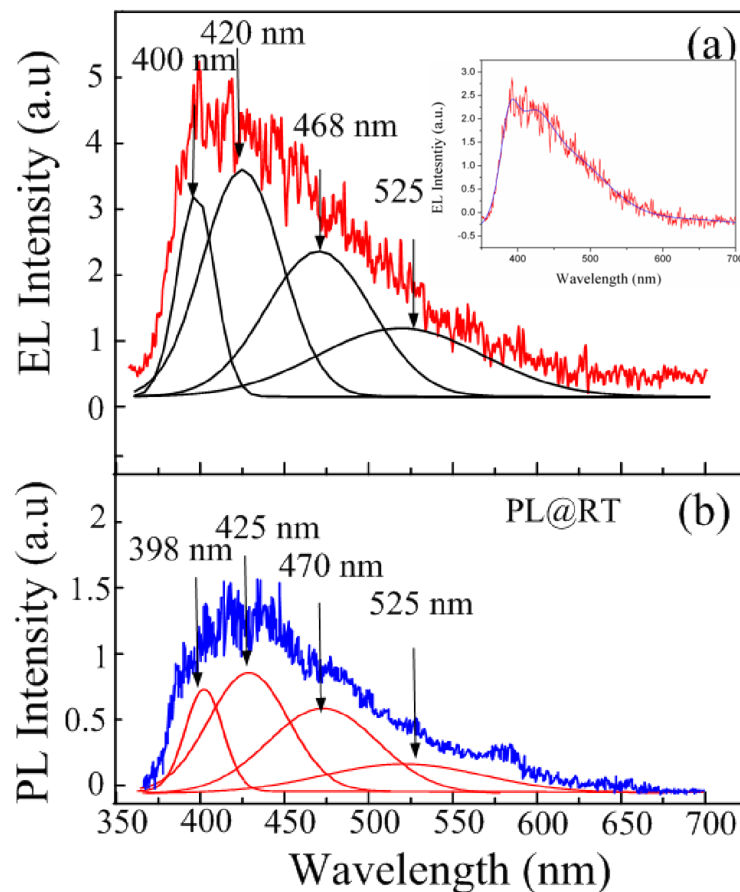

Fig. 6.5 EL spectrum with the fitting results of the LED under forward biased voltage of 14.6 V. The inset shows the sum of the four Gaussian peaks. (b) PL spectrum with the fitting results of the nanowires deposited on the *p*-SiC substrate.

It is generally believed that the visible emission of nanowires is originated from the surface oxygen defects due to their large surface to volume ratio. The oxygen impurities can produce defects including oxygen point defects, V_N and O_N-V_{Al} complexes to form

the deep levels or trap-level states inside the bandgap of the nanowires.[78,81] Hence, the visible emission may result from the radiative recombination between electrons occupying V_N and holes in the valance band.[58,82] It is also possible to have radiative transition between shallow levels of V_N and deep levels of O_N-V_{Al} complexes.[45,83] However, in order to explain the emission characteristics observed from both PL and EL spectra, it is necessary to have some trap-level states inside the bandgap contributing to both electrical and optical excitation processes. This can be interpreted in terms of energy-band diagram as shown below.

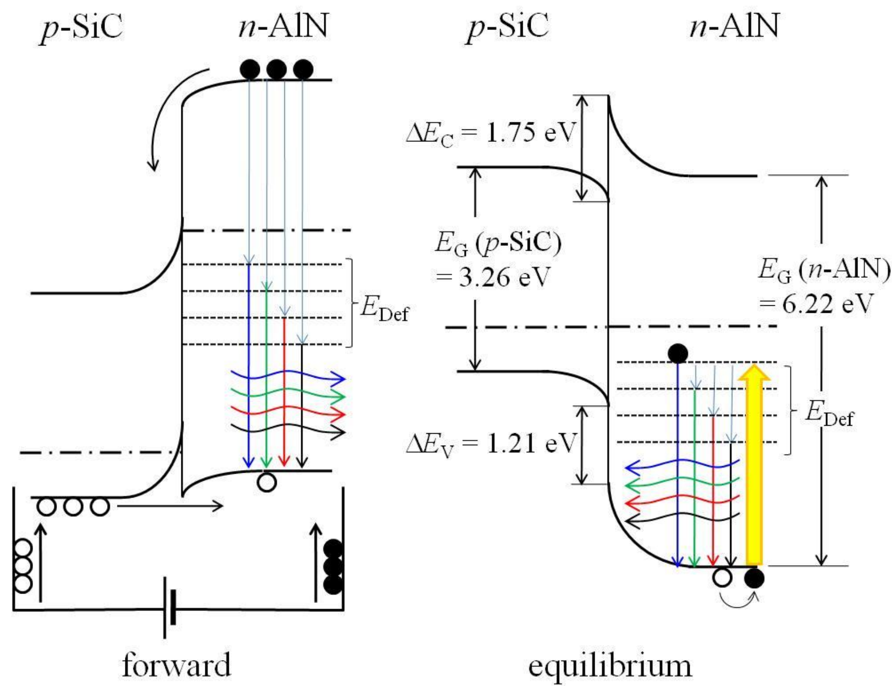

Fig. 6.6 Energy band diagrams for the heterojunction under forward bias and at equilibrium. E_{Def} represents the four trap-level states of the nanowires.

As mentioned above, four recombination centers are found from the nanowires. Fig. 6.6 shows the energy-band diagram of the heterojunction under forward bias and at equilibrium. As shown in figure 6.1 (d), the nanowires are in good contact with the *p*-SiC

substrate so that their vacuum levels can be roughly continued across the heterojunction. The electron affinity energies of nanowires and *p*-SiC are assumed to be ~2.30 and ~4.05 eV respectively.[84] Furthermore, the bandgap energy (E_g) of AlN is set to ~6.0 eV and that of the *p*-SiC [E_g (*p*-SiC)], is set to be ~3.26 eV. It can be shown that the conduction band offset, E_C and valance band offset E_V of the heterojunction are roughly equal to 1.75 and 1.21 eV respectively. The Fermi level of *p*-SiC substrate, according to its high hole concentration and carrier density, can be estimated to be ~0.5 eV above the valence band. Moreover, the Fermi level of nanowires is predicted to be ~2.4 eV below the conduction band. Since no Mg content can be detected from the nanowires as mentioned in chapter 4, the nanowires can be regarded as undoped AlN, which is intrinsically *n*-type. Because the difference between E_C and E_V is not large, holes can be injected from the valence band of *p*-SiC into that of nanowires under the forward bias. Electrons in the conduction band of the nanowires can then be relaxed non-radiatively to the four trap-level states with energies of E_{Def} and then radiatively recombined with holes in the valence band of the nanowires, see Fig. 6.6 (a). On the other hand, for the heterojunction under optical excitation, radiative recombination can be obtained from the photo-generated holes at the valence band with the excited electrons occupying the four trap-level states, see also Fig. 6.6 (b).

The four trap-level states as mentioned above are 398 nm (3.12 eV), 425 nm (2.92 eV), 470 nm (2.64 eV) and 525 nm (2.36 eV). The first trap-level state (3.12 eV) and second trap-level state (2.36 eV) are believed to be the nitrogen vacancies (V_N) recombines with the electron from the deep donor level. This phenomenon can be also observed in N

deficient AlN thin films and nanoparticle structures.[78] The nitrogen vacancy related peak can be ranging from 2 to 3.1 eV.[78]

The third trap-level state (2.92 eV) and fourth trap-level state (2.64 eV) are attributed to O_N emissions. This is because there were no active nitrogen sources for the growth of the nanowires. The N_2 gas only acted as the protection and carrier gas. Therefore, the formation of O_N is inevitable during the growth process.[85] This peak intensity can be successfully suppressed under the annealing of ammonia as confirmed by Qing Zhao.[82] Hence, this peak is very likely to be the emission peaks of nitrogen vacancy levels.

6.6 Summary

Randomly packed AlNNWs were synthesized on *p*-SiC to form a heterojunction LED. It is found that the growth direction of the AlNNWs grown on *p*-SiC substrate was different from that of the AlNNWs grown on sapphire substrate, which is along the [001] direction. A broad EL ad PL emissions centered at ~410 nm were obtained from the sample and EL emission can only be obtained under forward bias. The turn on voltage of the LED is 8 V, which is close to the bandgap of AlN (~6.0 eV). Although the *I*-*V* characteristic is not perfectly linear, the absolute voltage below 15 V is almost linear as observed from the relationship between *I* and *V* when measured on the top electrode.

It is found that the PL emission spectrum can be fitted by four Gaussian curves with peak wavelength at ~400, ~420, ~468 nm and ~525 nm. Therefore, the nanowires can be considered to have four radiative recombination centers. The origins of these recombination centers are believed to be the V_N and O_N defect trap-levels.

Chapter 7 Conclusion and Future Work

7.1 Conclusion

In this work, AlNNWs and zigzag AlNNWs were obtained using CVD method. The $MgCl_2$ powder was essential for the growth of the nanowires as no nanowires were obtained if $MgCl_2$ powder was not mixed with AlN powder. Therefore, it is believed that $MgCl_2$ acted as catalyst to initiate the growth of nanowires.

The growth temperature of the nanowires and zigzag nanowires were different. When the temperature was set at 1450 ^{o}C, the growth of the nanowires was favored, whereas the zigzag nanowires were favored at 1350 ^{o}C. These two kinds of nanowires possessed different structural properties. For the AlNNWs, no Mg was found from the EDX and the growth direction was along the [100] direction, which was the hexagonal *a*-axis of h-AlN. In contrast, about 5 at.% of Mg was found in the zigzag AlNNWs and the growth direction was along the [001] direction, which was the hexagonal *c*-axis of h-AlN. Moreover, shift of the Raman peaks to higher wavenumbers were observed from the zigzag nanowires due to the doping of Mg. Since Mg dopants were doped into the zigzag nanowires, room temperature ferromagnetism was detected from the zigzag AlNNWs with the spontaneous saturated magnetization and coercivity estimated to be ~0.5 μemu/mm^2 and 3 kOe respectively.

Due to the low vacuum condition during the growth process, all the samples were contaminated with oxygen from which no near bandedge emission were obtained. However, the AlNNWs and zigzag AlNNWs possessed different optical properties. For

the AlNNWs, a broad oxygen defect related emission peak centered at ~3.52 eV was obtained. The defect emission peak is believed to be attributed to the O_N level as the growth process of the nanowires was Al rich but lack of N as there was no active nitrogen source for the growth of nanowires. In contrast, oxygen related defect emission peak centered at ~3.46 eV was observed from the zigzag nanowires and a weak and broad emission peak centred at 4.7 eV was observed from the PL spectrum at 10 K. This emission peak is believed to be the transmission from the V_N^{3+} to the Mg^o. Generally, the zigzag AlNNWs had an emission peak located at lower energy when compared with the AlNNWs, which was believed to be due to the incorporation of Mg dopants as the Mg dopants could create deep acceptor level above the valence band of AlN.

Since the defect emission from the AlNNWs was quite stable and the yield of which was higher than zigzag AlNNWs, an AlNNWs/*p*-SiC heterojunction LED was fabricated. The growth direction of the nanowires grown on *p*-SiC substrate was different from that of the AlNNWs grown on sapphire substrate, which was along the [001] direction. A broad EL emission peak centered at 410 nm was observed from the LED. The turn on voltage of the LED was 8 V under the forward bias. Since no lights were observed under reversed bias, the rectifier obtained was originated by the heterojunction but not the Schottky barrier between the contact electrodes and the nanowires. The PL emission spectrum was able to fit by four Gaussian curves with peak wavelength at ~400, ~420, ~468 nm and ~525 nm. The origins of these recombination centers were believed to be the V_N and O_N related defect trap- levels.

7.2 Future Work

It is believed that oxygen defect has dominated the emission of the AlNNWs so that no near band emission can be obtained at room temperature. Therefore, the vacuum level and the choice of N source for the growth of AlNNWs are crucial. In order to synthesize nanowires with different dopant concentrations, the dopants should be able to place at different temperature zones.

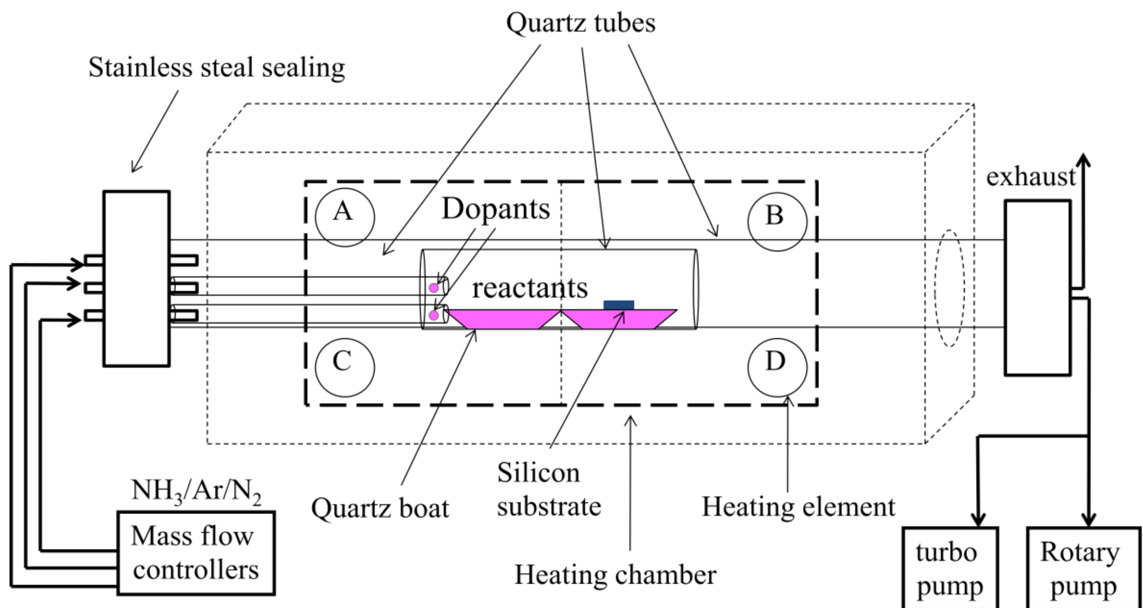

Fig. 7.1 Schematic diagram of the new horizontal tube furnace setup.

Therefore, a new tube furnace system is needed to grow AlNNWs with improved quality. In this setup, a turbo pump will be incorporated with the rotary pump so that the base vacuum for the growth can be as high as 10^{-5} Pa to prohibit the effect of oxygen contamination. The reactants will be replaced by $AlCl_3$ powder and a more reactive NH_3 gas so that the synthesis temperature can be lower.

All the outer and inner tubes will be replaced by quartz tubes due to their ability to sustain fast heating. Thus, the factor of heating rate can be eliminated for the growth of nanowires as the reactants will be loaded outside the heating region during the heat up process. The reactants will not be heated until the desired reaction temperature is attained. Once the reaction temperature is achieved, the whole outer quartz tube will be pushed to the center of the furnace to obtain the accurate heating time for the growth of nanowires.

Furthermore, the three inlet gas supplies will also be incorporated with two more inner quartz tubes such that at least two different dopants can be introduced into the reactants at one time, see fig. 7.1. It is hoped that the dopant concentrations can be tuned by varying the dopant positions and gas flows inside the inner quartz tubes and co-doped samples can be fabricated.

References

1 J. L. Spcier and S.M. Bradshaw, "Combustion Synthesis of Aluminum Nitride Particles and Whiskers," J. Am. Ceram. Soc. **82**, 2293 (1999).

2 S. Pearton and G. Fasol S. Nakamura, *The Blue Laser Diode: The Complete Story*. (Springer-Verlag, Berlin, 2000).

3 Y. Taniyasu, M. Kasu, and T. Makimoto, "An aluminium nitride light-emitting diode with a wavelength of 210 nanometres," Nature **441** (7091), 325-328 (2006).

4 S. Nikishin, B. Borisov, M. Pandikunta, R. Dahal, J. Y. Lin, H. X. Jiang, H. Harris, and M. Holtz, "High quality AlN for deep UV photodetectors," Applied Physics Letters **95**, 054101 (2009).

5 A. Samman, S. Gebremariam, L. Rimai, X. Zhang, J. Hangas, and G. W. Auner, "Platinum-aluminum nitride-silicon carbide diodes as combustible gas sensors," Journal of Applied Physics **87** (6), 3101-3107 (2000).

6 M. L. Nakarmi, N. Nepal, C. Ugolini, T. M. Altahtamouni, J. Y. Lin, and H. X. Jiang, "Correlation between optical and electrical properties of Mg-doped AlN epilayers," Applied Physics Letters **89** (15), 152120 (2006).

7 T. Kachi M. Kanechika, "n-type AlN layer by Si ion implantation," Appl. Phys. Lett. **88**, 202106 (2006).

8 Y. Taniyasu, M. Kasu, and T. Makimoto, "Electrical conduction properties of n-type Si-doped AlN with high electron mobility," Applied Physics Letters **85** (20), 4672-4674 (2004).

9 T. Kuykendall, P. J. Pauzauskie, Y. F. Zhang, J. Goldberger, D. Sirbuly, J. Denlinger, and P. D. Yang, "Crystallographic alignment of high-density gallium nitride nanowire arrays," Nature Materials **3** (8), 524-528 (2004).

10 Z. Liliental-Weber, D. N. Zakharov, K. M. Yu, J. W. Ager, W. Walukiewicz, E. E. Haller, H. Lu, and W. J. Schaff, "Compositional modulation in $In_xGa_{1-x}N$: TEM and X-ray studies," Journal of Electron Microscopy **54** (3), 243-250 (2005).

11 Y. P. Sun, Y. H. Cho, H. M. Kim, and T. W. Kang, "High efficiency and brightness of blue light emission from dislocation-free InGaN/GaN quantum well nanorod arrays," Applied Physics Letters **87** (9), 093115 (2005).

12 E. Ertekin, P. A. Greaney, D. C. Chrzan, and T. D. Sands, "Equilibrium limits of coherency in strained nanowire heterostructures," Journal of Applied Physics **97** (11), 114325 (2005).

13 M. Ben Ishai and F. Patolsky, "Shape- and Dimension-Controlled Single-Crystalline Silicon and SiGe Nanotubes: Toward Nanofluidic FET Devices," Journal of the American Chemical Society **131** (10), 3679-3689 (2009).

14 D. J. Sirbuly, M. Law, P. Pauzauskie, H. Q. Yan, A. V. Maslov, K. Knutsen, C. Z. Ning, R. J. Saykally, and P. D. Yang, "Optical routing and sensing with nanowire assemblies," Proceedings of the National Academy of Sciences of the United States of America **102** (22), 7800-7805 (2005).

15 H. Amano I. Akasaki, "Crystal gorwth and conductivity control of group III nitride semiconductors and their application to short wavelength light emitters," Japan Journal of Applied Physics **36**, 5393 (1997).

16 J. M. Bao, M. A. Zimmler, F. Capasso, X. W. Wang, and Z. F. Ren, "Broadband ZnO single-nanowire light-emitting diode," Nano Letters **6** (8), 1719-1722 (2006).

17 X. F. Duan, Y. Huang, R. Agarwal, and C. M. Lieber, "Single-nanowire electrically driven lasers," Nature **421** (6920), 241-245 (2003).

18 J. F. Wang, M. S. Gudiksen, X. F. Duan, Y. Cui, and C. M. Lieber, "Highly polarized photoluminescence and photodetection from single indium phosphide nanowires," Science **293** (5534), 1455-1457 (2001).

19 S. et al. Nakamura, "Superbright green InGaN SQW structure LEDs.," Jpn. J. Appl. **34**, L1332-L1335 (1995).

20 J. Han, M. H. Crawford, R. J. Shul, J. J. Figiel, M. Banas, L. Zhang, Y. K. Song, H. Zhou, and A. V. Nurmikko, "AlGaN/GaN quantum well ultraviolet light emitting diodes," Applied Physics Letters **73** (12), 1688-1690 (1998).

21 X. H. Ji, S. P. Lau, S. F. Yu, H. Y. Yang, T. S. Herng, A. Sedhain, J. Y. Lin, H. X. Jiang, K. S. Teng, and J. S. Chen, "Ultraviolet photoluminescence from ferromagnetic Fe-doped AlN nanorods," Applied Physics Letters **90** (19), 193118 (2007).

22 Y. Yang, Q. Zhao, X. Z. Zhang, Z. G. Liu, C. X. Zou, B. Shen, and D. P. Yu, "Mn-doped AlN nanowires with room temperature ferromagnetic ordering," Applied Physics Letters **90** (9), 092118 (2007).

23 L. B. Jiang, H. Li, S. B. Zuo, H. Q. Bao, W. J. Wang, and X. L. Chen, "Temperature dependence of Raman scattering in Co-doped AlN whiskers," Applied Physics a-Materials Science & Processing **100** (2), 545-550 (2010).

24 X. H. Ji, S. P. Lau, S. F. Yu, H. Y. Yang, T. S. Herng, and J. S. Chen, "Ferromagnetic Cu-doped AlN nanorods," Nanotechnology **18** (10), 105601 (2007).

25 R. Q. Wu, G. W. Peng, L. Liu, Y. P. Feng, Z. G. Huang, and Q. Y. Wu, "Ferromagnetism in Mg-doped AlN from ab initio study," Applied Physics Letters **89** (14), 142501 (2006).

26 Y. Li, F. Qian, J. Xiang, and C. M. Lieber, "Nanowire electronic and optoelectronic devices," Materials Today **9** (10), 18-27 (2006).

27 C. B. Murray, C. R. Kagan, and M. G. Bawendi, "Synthesis and characterization of monodisperse nanocrystals and close-packed nanocrystal assemblies," Annual Review of Materials Science **30**, 545-610 (2000).

28 J. M. Krans, J. M. Vanruitenbeek, V. V. Fisun, I. K. Yanson, and L. J. Dejongh, "The Signature of Conductance Quantization in Metallic Point Contacts," Nature **375** (6534), 767-769 (1995).

29 K. K. Likharev, "Layered tunnel barriers for nonvolatile memory devices," Applied Physics Letters **73** (15), 2137-2139 (1998).

30 G. Markovich, C. P. Collier, S. E. Henrichs, F. Remacle, R. D. Levine, and J. R. Heath, "Architectonic quantum dot solids," Accounts of Chemical Research **32** (5), 415-423 (1999).

31 Z. L. Wang, "Characterizing the structure and properties of individual wire-like nanoentities," Advanced Materials **12** (17), 1295 (2000).

32 P. Alivisatos, "Colloidal quantum dots. From scaling laws to biological applications," Pure and Applied Chemistry **72** (1-2), 3-9 (2000).

33 M. Nirmal and L. Brus, "Luminescence photophysics in semiconductor nanocrystals," Accounts of Chemical Research **32** (5), 407-414 (1999).

34 R. J. Shul, F. Ren, and E. Wolfgang, "Special issue - Power semiconductor devices and processes - Preface," Solid-State Electronics **42** (12), 2117-2117 (1998).

35 H. M. Huang, R. S. Chen, H. Y. Chen, T. W. Liu, C. C. Kuo, C. P. Chen, H. C. Hsu, L. C. Chen, K. H. Chen, and Y. J. Yang, "Photoconductivity in single AlN nanowires by subband gap excitation," Applied Physics Letters **96** (6), 062104 (2010).

36 J. Zheng, Y. Yang, B. Yu, X. B. Song, and X. G. Li, "[0001] oriented aluminum nitride one-dimensional nanostructures: Synthesis, structure evolution, and electrical properties," Acs Nano **2** (1), 134-142 (2008).

37 Y. B. Tang, H. T. Cong, and H. M. Cheng, "Field emission from honeycomblike network of vertically aligned AlN nanoplatelets," Applied Physics Letters **89** (9), 093113 (2006).

38 Zeitschr H. Ott, "Das Gitter des Aluminiumnitrids (AlN)," Physik **22** (1), 201-214 (1924).

39 J. Chem. Phys. G. A. Jeffrey and G. S. Parry, "Crystal structure of aluminum nitride," J. Chem. Phys. **23** (1953).

40 W. M. Yim, E. J. Stofko, Zanzucch.Pj, J. I. Pankove, Ettenber.M, and S. L. Gilbert, "Epitaxially Grown Aln and Its Optical Band Gap," Journal of Applied Physics **44** (1), 292-296 (1973).

41 G. A. Slack and T. F. Mcnelly, "Growth of High-Purity Ain Crystals," Journal of Crystal Growth **34** (2), 263-279 (1976).

42 A. Mitrushchenkov, G. Chambaud, J. Yvonnet, and Q. C. He, "Towards an elastic model of wurtzite AlN nanowires," Nanotechnology **21** (25), 255702 (2010).

43 R. H. Tredgold K. Kawabe, and Y. Inuishi, "Electrical and optical properties of AIN-A thermostable semiconductor," Electrt. Eng. Jpn. **87** (1967).

44 G. R. Yazdi, P. O. A. Persson, D. Gogova, R. Fornari, L. Hultman, M. Syvajarvi, and R. Yakimova, "Aligned AlN nanowires by self-organized vapor-solid growth," Nanotechnology **20** (49), 495304 (2009).

45 S. C. Shi, S. Chattopadhyay, C. F. Chen, K. H. Chen, and L. C. Chen, "Structural evolution of AlN nano-structures: Nanotips and nanorods," Chemical Physics Letters **418** (1-3), 152-157 (2006).

46 J. Edwards, K. Kawabe, G. Stevens, and R. H. Tredgold, "Space charge conduction and electrical behaviour of aluminium nitride single crystals," Solid State Communications **3**, 99 (1965).

47 Y. Taniyasu, M. Kasu, and T. Makimoto, "Heterostructure growth of a single-crystal hexagonal AlN (0001) layer on cubic diamond (111) surface," Applied Physics Letters **108**, 013528 (2010).

48 K. B. Nam, J. Li, M. L. Nakarmi, J. Y. Lin, and H. X. Jiang, "Deep ultraviolet picosecond time-resolved photoluminescence studies of AlN epilayers," Applied Physics Letters **82** (11), 1694-1696 (2003).

49 J. Li, K. B. Nam, M. L. Nakarmi, J. Y. Lin, and H. X. Jiang, "Band-edge photoluminescence of AlN epilayers," Applied Physics Letters **81** (18), 3365-3367 (2002).

50 M. Strassburg, J. Senawiratne, N. Dietz, U. Haboeck, A. Hoffmann, V. Noveski, R. Dalmau, R. Schlesser, and Z. Sitar, "The growth and optical properties of large, high-quality AlN single crystals," Journal of Applied Physics **96** (10), 5870-5876 (2004).

51 G. A. Cox, D. O. Cummins, K. Kawabe, and R. H. Tredgold, "Properties and Electrical Behavior of Aluminum Nitride," Journal of Physics and Chemistry of Solids **28**, 543 (1967).

52 S. L. Yang, R. S. Gao, P. L. Niu, and R. H. Yu, "Room-temperature ferromagnetic behavior of cobalt-doped AlN nanorod arrays," Applied Physics a-Materials Science & Processing **96** (3), 769-774 (2009).

53 B. I. Berger, "Semiconductor materials," CRC Press, 123 (1997).

54 M. S. Gudiksen, J. F. Wang, and C. M. Lieber, "Size-dependent photoluminescence from single indium phosphide nanowires," Journal of Physical Chemistry B **106** (16), 4036-4039 (2002).

55 X. H. Ji, Q. Y. Zhang, Z. Y. Ling, and S. P. Lau, "Stress and its effect on optical properties of AlN nanorods," Applied Physics Letters **95** (23), 233105 (2009).

56 X. H. Ji, Q. Y. Zhang, S. P. Lau, H. X. Jiang, and J. Y. Lin, "Temperature-dependent photoluminescence and electron field emission properties of AlN nanotip arrays," Applied Physics Letters **94** (17), 173106 (2009).

57 H. Ohno, "Making nonmagnetic semiconductors ferromagnetic," Science **281** (5379), 951-956 (1998).

58 Y. B. Tang, "Synthesis and properties of one-diemensional aluminum nitride nanostructures," Nano Letters **2** (6), 307 (2007).

59 R. S. Wagner and W. C. Ellis, "VAPOR-LIQUID-SOLID MECHANISM OF SINGLE CRYSTAL GROWTH," Applied Physics Letters **4**, 89 (1960).

60 S. C. Shi, C. F. Chen, S. Chattopadhyay, Z. H. Lan, K. H. Chen, and L. C. Chen, "Growth of single-crystalline wurtzite aluminum nitride nanotips with a self-selective apex angle," Advanced Functional Materials **15** (5), 781-786 (2005).

61 Y. B. Tang, H. T. Cong, Z. M. Wang, and H. M. Cheng, "Catalyst-seeded synthesis and field emission properties of flowerlike Si-doped AlN nanoneedle array," Applied Physics Letters **89** (25), 253112 (2006).

62 Q. Wu, Z. Hu, X. Z. Wang, Y. M. Hu, Y. J. Tian, and Y. Chen, "A simple route to aligned AlN nanowires," Diamond and Related Materials **13** (1), 38-41 (2004).

63 William Clegg, *Crystal structure determination*. (Oxford University Press, Oxford ; New York, 1998).

64 Carmelo Giacovazzo, *Fundamentals of crystallography*. (International Union of Crystallography; Oxford University Press, Oxford ; New York, 1992).

65 Joseph Goldstein, *Scanning electron microscopy and X-ray microanalysis : a text for biologists, materials scientists, and geologists*. (Plenum Press, New York, 1992), 2nd ed.

66 R. M. Anderson and Scott D. Walck, *Specimen preparation for transmission electron microscopy of materials IV : symposium held April 2, 1997, San Francisco, California, U.S.A.* (Materials Research Society, Pittsburgh, Pa., 1997).

67 Peter Buseck, J. M. Cowley, and LeRoy Eyring, *High-resolution transmission electron microscopy and associated techniques*. (Oxford University Press, New York, 1988).

68 Arnold Gucsik, *Cathodoluminescence and its application in the planetary sciences*. (Springer, Berlin, 2009).

69 Lyuji Ozawa, *Cathodoluminescence and photoluminescence : theories and practical applications*. (CRC Press, Boca Raton, 2007).

70 http://www.oceanoptics.com/, "Detector spectrum", (Ocean Optics, Hong Kong, 2010).

71 J. A. Haber and W. E. Buhro, "Kinetic instability of nanocrystalline aluminum prepared by chemical synthesis; Facile room-temperature grain growth," Journal of the American Chemical Society **120** (42), 10847-10855 (1998).

72 P. Ulrich T. Kutkendall, S. Aloni and P. Yang, "Complete composition tunability of InGaN nanowires using a combinatorial approach," Nature Materials **6**, 951 (2007).

73 J. Zheng, X. B. Song, B. Yu, and X. G. Li, "Asymmetrical AlN nanopyramids induced by polar surfaces," Applied Physics Letters **90** (19), 193121 (2007).

74 L. H. Shen, X. F. Li, Q. L. Cui, B. B. Liu, and T. Cui, "Formation and growth mechanism of ripple-like AlN nanowires," Applied Physics a-Materials Science & Processing **99** (1), 111-115 (2010).

75 H. Wu, R. Zheng, W. Liu, S. Meng, and J. JHuang, "C and Si codoping method for p-type AlN," Journal of Applied Physics **108**, 053715 (2010).

76 H. T. Wang, Z. P. Xie, Y. G. Wang, W. Y. Yang, Q. F. Zeng, F. Xing, and L. N. An, "Single-crystal AlN nanonecklaces," Nanotechnology **20** (2), 025611 (2009).

77 H. J. Fan, M. Knez, R. Scholz, K. Nielsch, E. Pippel, D. Hesse, U. Gosele, and M. Zacharias, "Single-crystalline $MgAl_2O_4$ spinel nanotubes using a reactive and removable MgO nanowire template," Nanotechnology **17** (20), 5157-5162 (2006).

78 T. Mattila and R. M. Nieminen, "Ab initio study of oxygen point defects in GaAs, GaN, and AlN," Physical Review B **54** (23), 16676-16682 (1996).

79 C. Yuen, S. F. Yu, S. P. Lau, Rusli, and T. P. Chen, "Fabrication of n-ZnO : Al/p-SiC(4H) heterojunction light-emitting diodes by filtered cathodic vacuum arc technique," Applied Physics Letters **86** (24), 241111 (2005).

80 B. Bastek, F. Bertram, J. Christen, T. Hempel, A. Dadgar, and A. Krost, "Analysis of point defects in AlN epilayers by cathodoluminescence spectroscopy," Applied Physics Letters **95** (3), - (2009).

81 R. A. Youngman and J. H. Harris, "Luminescence Studies of Oxygen-Related Defects in Aluminum Nitride," Journal of the American Ceramic Society **73** (11), 3238-3246 (1990).

82 Q. Zhao, S. Q. Feng, Y. W. Zhu, X. Y. Xu, X. Z. Zhang, X. F. Song, J. Xu, L. Chen, and D. P. Yu, "Annealing effects on the field emission properties of AlN nanorods," Nanotechnology **17** (11), S351-S354 (2006).

83 C. Liu, Z. Hu, Q. Wu, X. Z. Wang, Y. Chen, H. Sang, J. M. Zhu, S. Z. Deng, and N. S. Xu, "Vapor-solid growth and characterization of aluminum nitride nanocones," Journal of the American Chemical Society **127** (4), 1318-1322 (2005).

84 J. Choi, R. Puthenkovilakam, and J. P. Chang, "Band structure and alignment of the AlN/SiC heterostructure," Applied Physics Letters **86** (19), 192101 - 192103 (2005).

85 G. A. Slack, L. J. Schowalter, D. Morelli, and J. A. Freitas, "Some effects of oxygen impurities on AlN and GaN," Journal of Crystal Growth **246** (3-4), 287-298 (2002).